J. Earth Sci. Nagoya Univ., Vol. 38, 11 to 38, 1991

The Chemical Th-U-total Pb Isochron Ages of Zircon and Monazite from the Gray Granite of the Hida Terrane, Japan

Kazuhiro SUZUKI and Mamoru ADACHI

Department of Earth Sciences, School of Science,
Nagoya University, Nagoya 464-01, Japan
(Received November 6, 1991)

ABSTRACT

Zircon and monazite from thirteen "Gray Granite" samples in the central part of the Hida terrane were analyzed precisely on an electron microprobe. The U-Th-Pb relation of zircon was examined in terms of PbO and UO_2* (UO_2* means measured UO_2 plus UO_2 equivalent of measured ThO_2), and that of monazite in terms of PbO and ThO_2* (measured ThO_2 plus ThO_2 equivalent of measured UO_2). Most zircon grains from the Gray Granite form euhedral prisms with concentric growth zones; only a few exhibit rounded and/or overgrowth forms. Analytical data for clear portions of euhedral zircon grains from individual samples are arrayed linearly on the PbO-UO_2* diagram and form a single isochron. The chemical Th-U-total Pb isochron ages of zircon are in the range from 230±10 to 250±20 Ma. Several zircon grains have rounded cores of Precambrian age (as old as 1270 Ma), suggesting contributions of recycled older materials to the formation of the Gray Granite. Monazite, recognized only in one sample, gives a chemical Th-U-total Pb isochron age of 230±10 Ma. These zircon and monazite ages strikingly contrast to previously measured Rb-Sr whole-rock isochron ages of 506±37 Ma for the Gray Granite (Shibata et al., 1989). Our microprobe observation of Sr- and Rb-distribution in granite samples discloses that the Gray Granite was open with respect to these elements during chloritization of biotite and sericitization of plagioclase. Consequently, the 506 Ma Rb-Sr isochron age as well as several Precambrian Rb-Sr model ages for the Gray Granite appears to be incorrect. Rather, we believe that the Gray Granite was emplaced into the Hida gneiss in early Triassic time (ca. 240 Ma).

INTRODUCTION

The Hida terrane occupying the northern part of Southwest Japan is one of pre-Cretaceous terranes in the Japanese Islands (e.g. Ichikawa, 1990). It consists of a variety of gneisses, schists, and granitoids (Suwa, 1990); which are unconformably overlain by the Jurassic-Cretaceous Tetori Group. Although extensive field, petrological, and geochronological investigations have been done on these rocks, the history of the Hida terrane is still unclear. The main point of arguments on the Hida terrane is whether or not it is composed of true Precambrian metamorphic and igneous rocks. Up to now, only the following four facts have received general consensus: (1) Among the granitoids, the Funatsu granitic rocks are the most widespread and were intruded in Jurassic time (ca. 180 Ma, Shibata and Nozawa, 1984), (2) Most of the metamorphic rocks are of the amphibolite facies and their radiometric ages concentrate around 240 Ma and 180 Ma (see the compilation of Ota and Itaya, 1989); no age data to indicate the Precambrian metamorphism have been obtained, (3) The Unazuki schists distributed in the eastern Hida terrane formed in Triassic time from upper Carboniferous to Permian sediments (Hiroi et al., 1978), and (4) A middle Precambrian $^{206}Pb/^{207}Pb$ age of 1493 Ma (dated for detrital grains of zircon in a gneiss sample from Amo, Ishizaka and Yamaguchi, 1969) shows that recycled Precambrian materials are present in some gneisses of the Hida terrane.

In the central part of the Hida terrane the so-called Gray Granite occurs as veins and dikes cutting the Hida gneisses. These bodies are too small to be shown on the geological map. The Gray Granite is characterized by bluish-tint K-feldspars which distinguish it from the Jurassic Funatsu granitic rocks. Sato et al. (1967) reported three preliminary Rb-Sr model ages from the Gray Granite at Futatsuya, about 5 km north of Kamioka (Fig. 1); 680 Ma for biotite, 810 Ma for microcline and 1200 Ma for whole-rock. Although these ages have never been confirmed, the age data coupled with the mode of

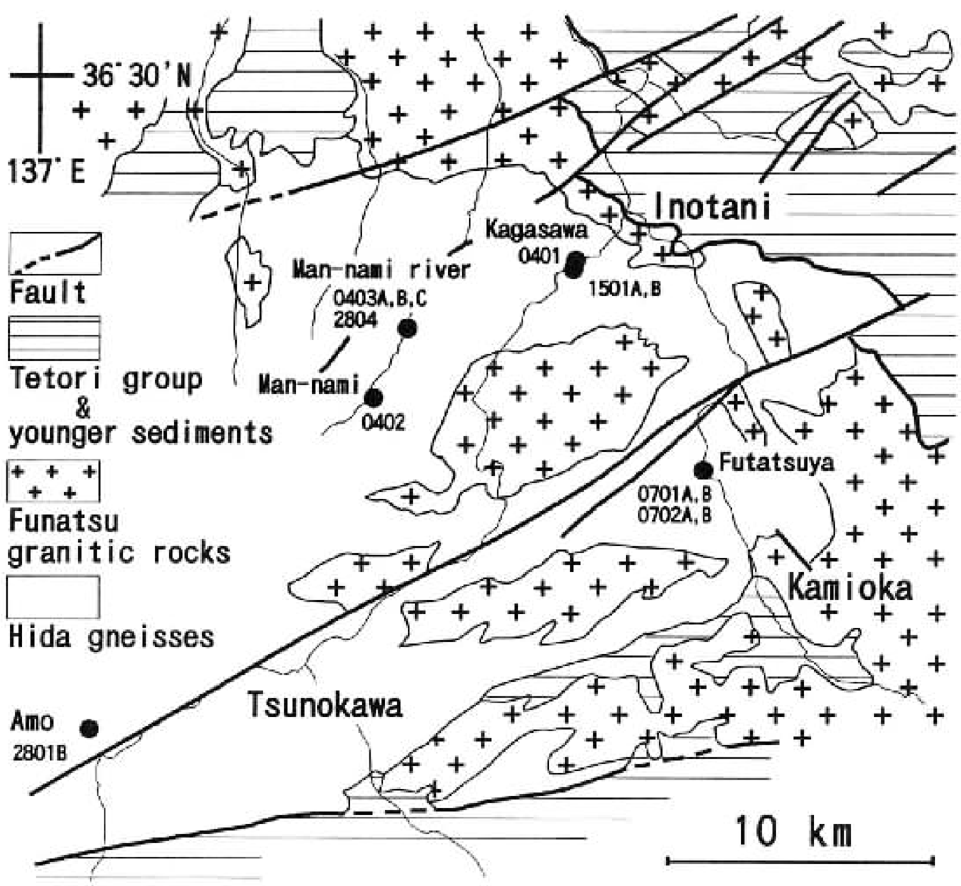

Fig. 1. Simplified geological map with sample localities of the Hida terrane in the central Japan (slightly modified from Kano, 1982).

occurrence of the Gray Granite have supported the idea that the Hida gneisses are of polymetamorphosed Precambrian origin (e.g. Sato, 1968; Suwa, 1969; Suzuki, 1977). Recently, Shibata and Nozawa (1986) reported ca. 1100 Ma and 700 Ma Rb-Sr model ages for two varieties of Gray Granite at Kagasawa (Fig. 1). Shibata et al. (1989) reported a Rb-Sr whole-rock isochron age of 506±37 Ma for the Gray Granite in the Kubusu River area (Man-nami River, Fig. 1). They demonstrated that the isochron age indicates an upper limit for the time of the Hida metamorphism. However, since their Rb-Sr isotopic data exhibit a significantly large scatter, we consider that the 506 Ma isochron age is inconclusive. To check the existence of the 506 Ma granitic veins and dikes as well as "Precambrian" Gray Granite by an alternative method, we have studied zircon and monazite from thirteen Gray Granite samples on an electron microprobe. Precise microprobe analyses of Th, U and Pb of zircon and monazite grains give us reliable geochronological information (Suzuki et al., 1991; Suzuki and Adachi, 1991).

GEOLOGIC SETTING AND SAMPLE DESCRIPTION

The metamorphic rocks in the central part of the Hida terrane are composed mainly of quartzo- feldspathic gneiss and crystalline limestone with subordinate amphibolite, pelitic gneiss and lime-silicate gneiss. The Gray Granite occurs as well-defined veins and dikes, usually several cm to ca. 2 m thick, in the Hida gneisses (Plates I-III).

Thirteen Gray Granite samples were collected from five localities (Fig. 1), Futatsuya (36°22'18", 137°16'40": Sample Nos. 0701A and 0701B; 36°22'20", 137°16'41": 0702A and 0702B), Kagasawa (36°26'8", 137°13'16" : Sample Nos. 1501A and 1502A; 36°26'25"N, 137°13'21"E: Sample No. 0401), Man-nami (36°23'46"N, 137°8'30"E: Sample No. 0402), Man-nami River (a tributary of the Kubusu River, 36°25'44"N, 137°9'28"E: Sample Nos. 0403A, 2804, 0403B and 0403C) and Amo (36°16'51"N, 137°0'44"E: Sample No. 2801B).

Most samples are of medium-to coarse-grained granite, quartz monzonite and granodiorite, but 0702A and 0403B samples are of pegmatite and 0701A, 1501A and 0403C samples are of pegmatitic granite to quartz monzonite. All samples consist mainly of quartz, cryptoperthite-perthite, plagioclase (mainly oligoclase in composition) and biotite with or without muscovite. Hornblende is rare. Plagioclase is occasionally sericitized and biotite, except for that contained in quartz is highly chloritized. Epidote and calcite are not uncommon especially in highly sericitized samples. Accessories include zircon, allanite, apatite, titanite and garnet. One sample (No. 0702B) contains thorite, and 1501B sample contains monazite but lacks titanite.

EXPERIMENTAL METHODS

Zircon and monazite for the present study were separated from samples of 2-3 kg. The size reduction of samples was undertaken on a stamp mill only to the extent necessary for disaggregation of zircon and monazite through periodic sieving to remove undersized (minus 80 mesh) particles before further reduction of oversized ones. From each sieved sample, we concentrated zircon, monazite and other heavy minerals with a pan. The concentrates were washed with dilute HCl and purified on an isodynamic magnetic separator. Zircon and monazite grains were hand-picked, mounted on a glass slide with epoxy resin, and polished with diamond paste until the grains were thinned approximately to half in thickness.

Zircon and monazite were analyzed on a JEOL JXA-5A electron microprobe equipped with three wavelength dispersive-type spectrometers. The operating conditions were 15 kV accelerating voltage, 0.02-0.15 μA probe current and 5 μm probe diameter. Analyzing crystals were TAP, PET and LiF crystals. The comparison standards were euxenite provided by Smellie et al. (1978) for Th and U, synthesized glass (56.17 % PbO, 13.65 % ZnO and 30.18 % SiO_2, analyst: H. Haramura, University of Tokyo) for Pb, synthesized glasses of Drake and Weill (1972) for Y and rare earths, and natural minerals

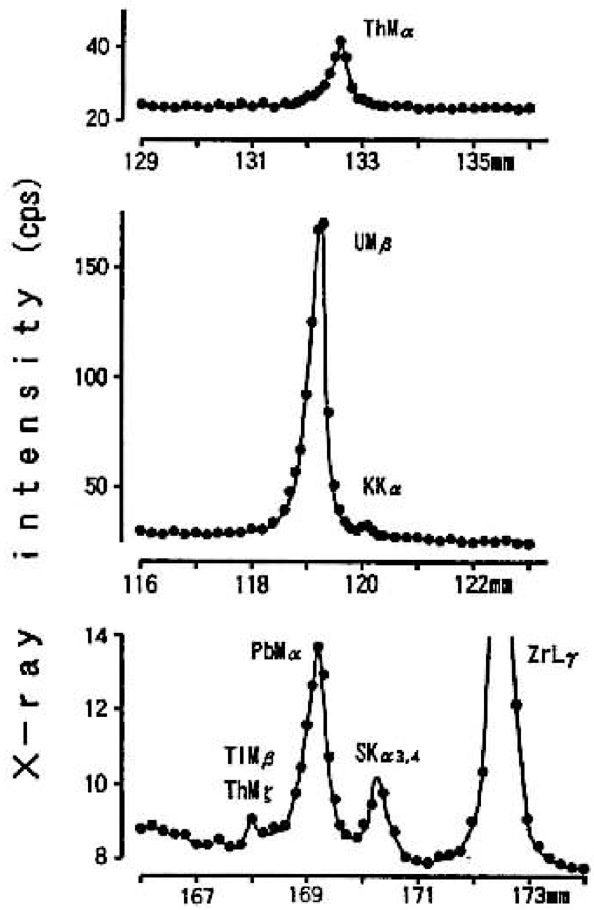

Fig. 2. X-ray emission spectra around the ThMα, UMβ and PbMα regions obtained through the pulse-height discriminator from spot 2 of Z03 zircon grain in 0403A sample. The ordinate represents X-ray intensity (cps) and the scale of abscissa represents the X-ray detection position (mm) of the JEOL spectrometer. The ThMα intensity is ca. 25 cps for 0.277 wt. % ThO_2 on a background intensity of ca. 24 cps, the UMβ intensity is ca. 150 cps for 2.05 wt. % UO_2 on a 25 cps background, the and the PbMα intensity is ca. 5 cps for 680 ppm PbO on a 9 cps background.

and synthesized oxides for other elements. The M-lines were used in the Th, U, Pb analysis; they give satisfactory intensities (Fig. 2). Spectral interferences including YLγ on PbMα were corrected through the procedure described by Amli and Griffin (1975). X-ray intensities of ThMα, UMβ and PbMα were integrated for 200 or 400 seconds. The measurement was repeated twice or three times, and the arithmetic average was taken. Raw intensity data were corrected for drift, background, dead time, atomic number, absorption and fluorescence. The detection limits of PbO at 2σ confidence level is 0.005-0.008 wt.%, and the relative error in the determination is about 5% for 0.1 wt.% and 10-15% for 0.02 wt.% of the concentration.

Age was calculated through the chemical Th-U-total Pb isochron method (CHIME; Suzuki et al., 1991; Suzuki and Adachi, 1991). Details of CHIME are shown in Appendix 1 for convenience.

RESULTS

The UO_2, ThO_2 and PbO analytical data and apparent ages are given in Appendix 2, and the PbO-UO_2* (ThO_2*) plots are shown in Figs. 3 to 11.

0701A: Futatsuya

This sample was collected from a ca. 10 cm thick vein of pegmatitic granite exposed along the Takahara River at Futatsuya (Plate I). The vein cuts subconcordantly the surrounding biotite gneiss. Zircon grains form euhedral prisms of 0.14-0.38 mm in length and 0.04-0.12 mm in width, and show concentric growth zoning (Plate IV-A). Some grains, however, exhibit rounded forms (Plate IV-B). Most zircon grains show low UO_2 and PbO contents, but several grains contain measurable amounts of UO_2 and PbO, 0.3-1.0 and 0.010-0.044 %, respectively. The ThO_2 contents are usually smaller than 0.1 %, but attain 2.4 % at rims of U-rich grains. The data points (solid circles) for core portions of euhedral grains are arrayed linearly in the PbO-UO_2* diagram (Fig. 3). These data points yield an isochron (MSWD=0.29) of 240±20 Ma with an intercept value of 0.0001±0.0016 (errors quoted in this paper for ages and intercept values are of 2σ). Two data points (open circles) for Th-rich rims do not show the same tendency as those for cores, but are plotted in an area below the 240 Ma isochron.

0701B: Futatsuya

This sample was collected from another vein that cuts nearly perpendicularly the biotite gneiss and the above-mentioned pegmatitic vein in the same outcrop as 0701A sample (Plate I). This vein, ca. 5 cm in width, consists of fine-grained quartz monzonite. Zircon occurs as euhedral prisms of 0.09-0.35 mm in length. Several grains, however, show rounded to subrounded forms. The ThO_2 contents rise up to 0.92 % and the UO_2 contents up to 1.04 %. Data points (solid triangles) for euhedral grains give an isochron of 250±20 Ma (MSWD=0.25) with an intercept value of -0.0003±0.0014 (Fig. 3). Three data points (open triangles) for rims of euhedral grains are plotted below the 250 Ma isochron, and the data point (square) for Z23 rounded grain is plotted above the isochron.

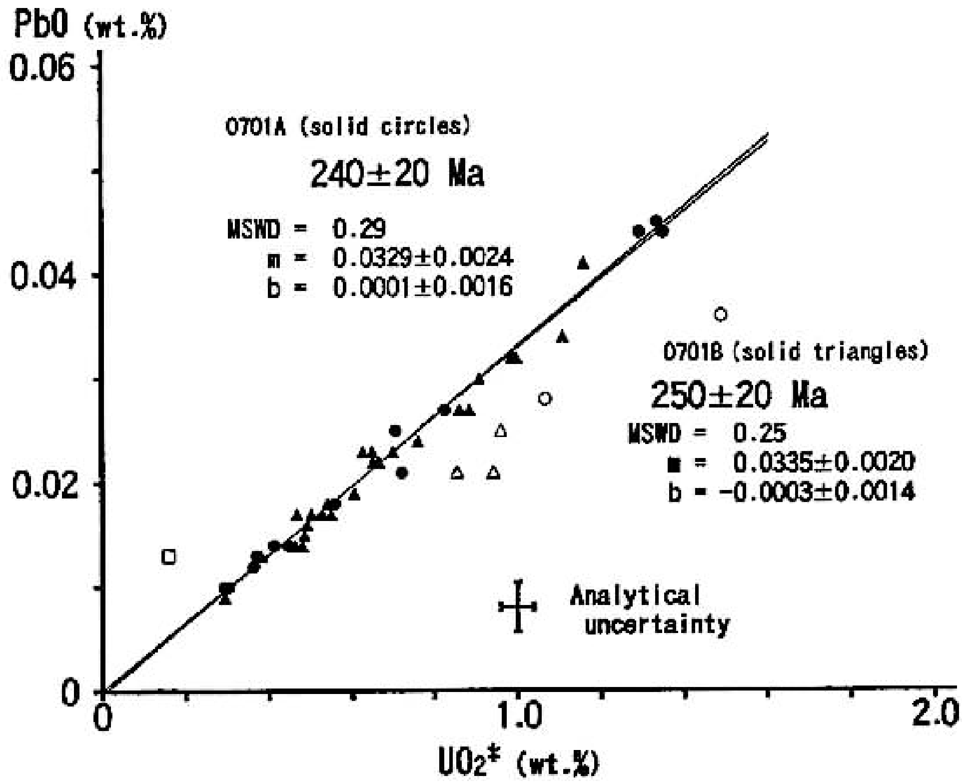

Fig. 3. Plot of PbO vs. UO_2* for zircon grains in 0701A and 0701B samples from Futatsuya. 0701A: solid circles represent data points for transparent portions of euhedral grains, and open circles represent data points for Th-rich rims. 0701B: solid triangles represent data points for transparent portions of euhedral grains, open triangles represent for rims of euhedral grain, and square for the core of a rounded zircon grain. Error bars in the figure represent 2σ analytical uncertainty, and errors referred for the age, slope (m) and intercept (b) are of 2σ .

0702A: Futatsuya

This sample was collected from a pegmatitic part of a ca. 20 cm thick vein at Futatsuya, about 60 m downstream from the outcrop for 0701A and 0701B samples. Zircon forms euhedral elongated crystals (0.31-0.43 mm in length and 0.08-0.16 mm in width), and displays concentric growth zoning. The ThO_2 contents of analyzed grains range from 0.16 to 5.77 %, the UO_2 contents from 0.25 to 2.44 %, and the PbO contents from 0.010 to 0.136 %. Most data points (solid circles) are arrayed linearly on the PbO-UO_2 diagram (Fig. 4), and give an isochron age of 240±10 Ma (MSWD=0.22) with an intercept value of -0.0001±0.0010. Three data points (open circles) for rims of Z03 and Z16 grains are plotted below the 240 Ma isochron, and one data point (square) for Z17 subrounded grain is plotted above the isochron.

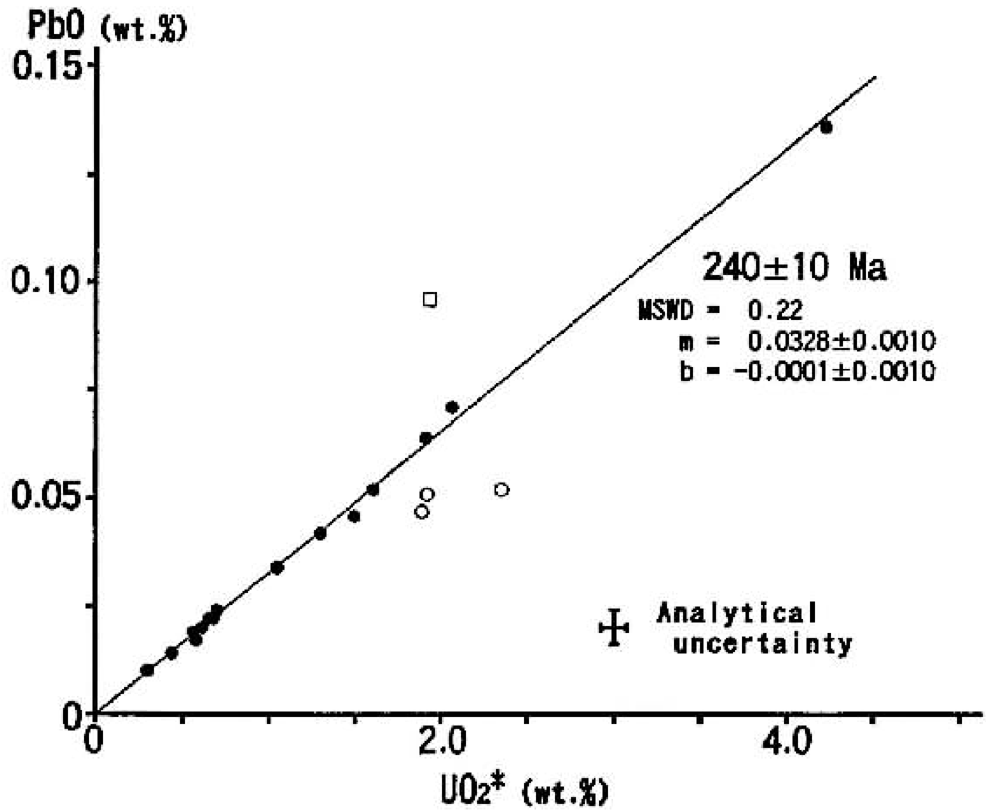

Fig. 4. Plot of PbO vs. UO_2* for zircon grains in 0702A sample from Futatsuya. Solid circles represent data points for transparent portions of euhedral grains, open circles represent for rims of Z03 and Z16 euhedral grain, and square for the core of Z17 rounded zircon grain. Explanation for errors is the same as Fig. 3.

0702B: Futatsuya

This sample was collected from a network vein that agmatized the hornblende-bearing biotite gneiss in the same outcrop as 0702A sample (Plate II). Unlike the other Gray Granite samples, this sample contains thorite and hornblende. Most zircon grains, 0.17-0.36 mm in length and 0.08-0.14 mm in width, exhibit euhedral form with concentric growth zoning, and some grains show a distinct core-overgrowth relation. The cores of core-overgrowth grains are well-rounded (Plate IV-C) to subrounded (Plates V-A and V-B), suggesting abrasion during transportation and/or metamorphic corrosion. The overgrown rims are euhedral, show concentric zoning as the result of magmatic crystallization, and have the same optical orientation as that for cores. The rounded detrital cores are higher in the Th and U contents than the overgrown rims; the core (Z03-01) of Z03 grain, for example, shows 31.9 % SiO_2, 61.5 % ZrO_2, 1.92 HfO_2, 1.53 % ThO_2, 1.25 % UO_2, 1.51 % Y_2O_3, 0.031 % Yb_2O_3, 0.303 % PbO and 0.339 % P_2O_5, whereas the rim (Z03-03) shows 32.5 % SiO_2, 64.6 % ZrO_2, 2.04 % HfO_2, 0.168 % ThO_2, 0.376 % UO_2, 0.192 % Y_2O_3, 0.009 % PbO and 0.095 % P_2O_5. The chemical composition of the overgrown rims does not differ from that of the euhedral grains. Analytical data of zircon are summarized in

Fig. 5. Most data points (solid circles) for euhedral grains and mantles of heterogeneous core-overgrowth grains give an isochron of 240±10 Ma (MSWD=0.82) and an intercept value of -0.0002±0.0014. Analytical data for cores of c ore-overgrowth grains Z03 (solid squares), Z16 (crosses) and Z14 (triangles) yield isochrons of 1270±80 Ma, 500±50 Ma and 340±20 Ma, respectively. Data points (open squares) for the cores of other core-overgrowth grains fall around the 500 and 340 Ma isochrons.

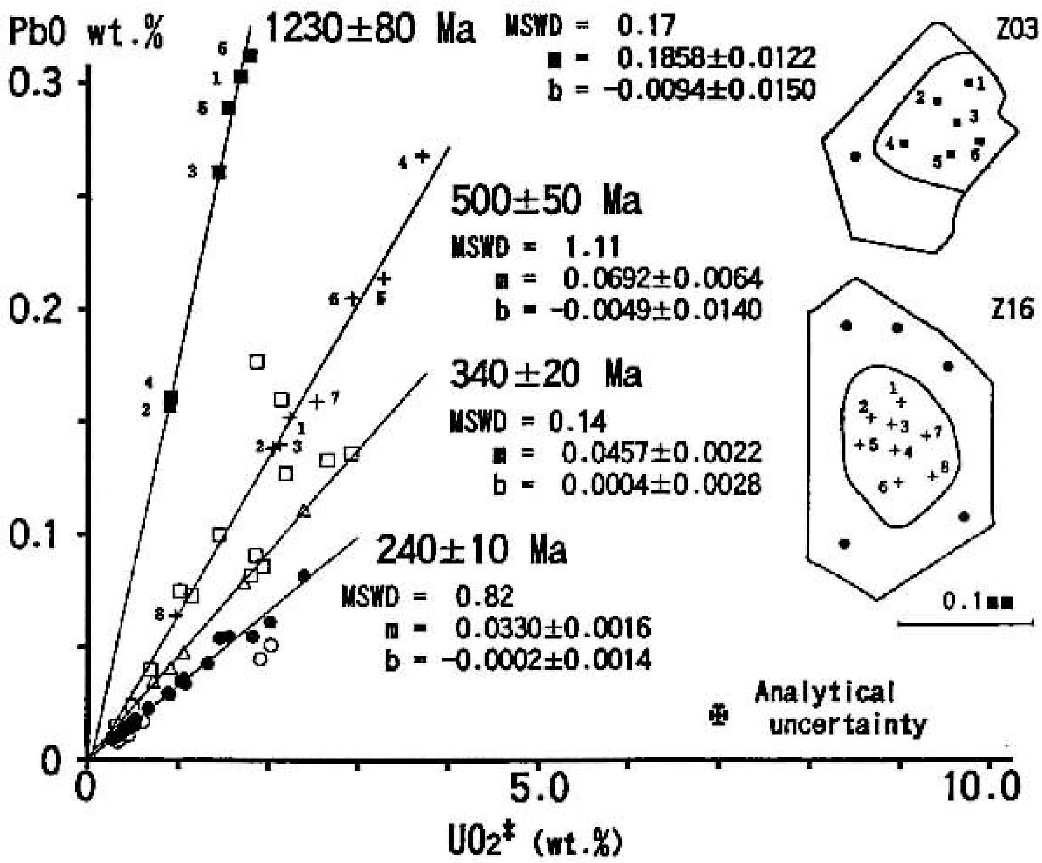

Fig. 5. Plot of PbO vs. UO_2* for zircon grains and cross sections of zircon grains Z03 and 16 showing analyzed spots in 0702B sample from Futatsuya. Solid circles represent data point for portions with concentric growth zoning, open circles for rims of euhedral zircon grains, open squares for cores of zircon grains with distinct core-overgrowth relations. Data points for cores of Z03 (solid squares) and Z16 (crosses) core-overgrowth grains are labeled, and those for the core of Z14 core-overgrowth grain are marked with triangles. Explanation for errors is the same as Fig.3.

1501A: Kagasawa

This sample was collected from the pegmatitic part of a ca. 50 cm thick network-vein in the hornblende-bearing biotite gneiss (Plate III). Shibata and Nozawa (1986) described this vein-rock as coarse-grained granite, carried out three Rb-Sr whole-rock analyses, and obtained 1090-1130 Ma Rb-Sr model ages taking an initial $^{87}Sr/^{86}Sr$ ratio of 0.704. Zircon grains form euhedral prisms of 0.20-0.40 mm in length and 0.11-0.17 mm in width, and have concentric growth zones. They contain 0.02-4.8 % ThO_2 and 0.2-5.2 % UO_2. The PbO content varies from less than the detection limit to 0.19 %. Analytical data (solid circles) for transparent portions of euhedral crystals define an isochron (MSWD= 0.32) of 240±10 Ma with an intercept value of 0.0005±0.0008 (Fig. 6). Three data points (open circles) for metamict rims are plotted below the 240 Ma isochron.

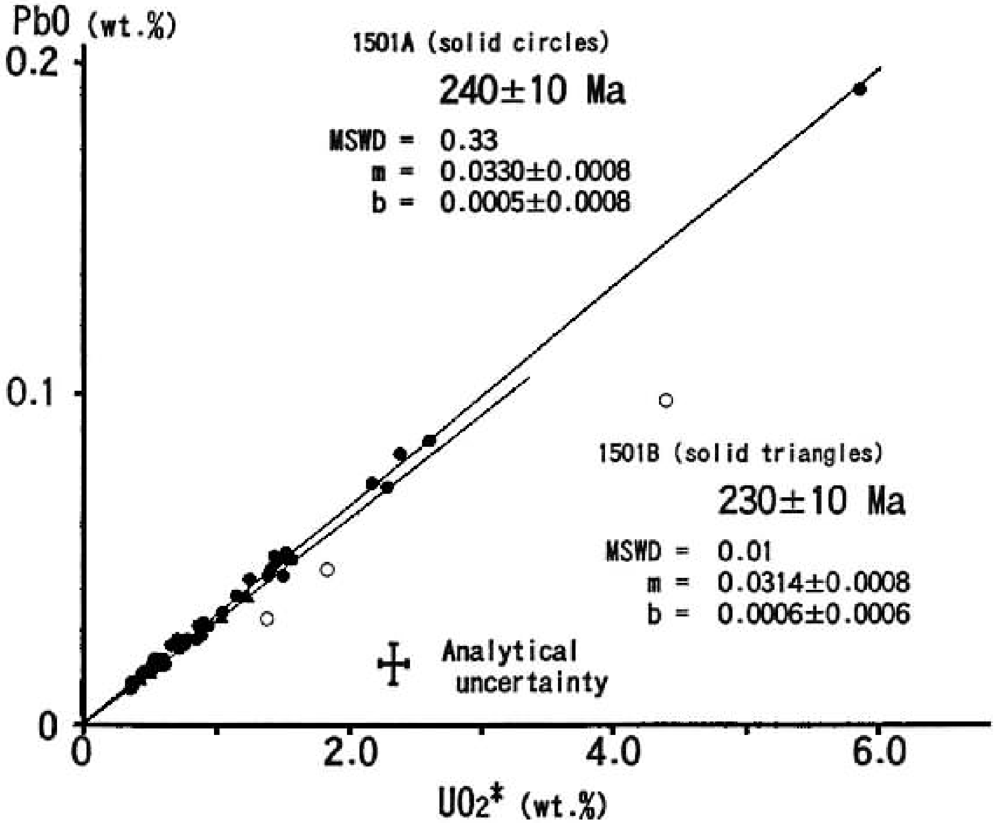

Fig. 6. Plot of PbO vs. UO_2* for zircon grains in 1501A and 1501B samples from Kagasawa. 1501A: solid circles represent data points taken for core portions of euhedral grains, and open circles represent data points for rims. 1501B: microprobe analyses were carried out only for transparent portions of euhedral grains (solid triangles). Explanation for errors is the same as Fig. 3.

1501B: Kagasawa

This sample was collected from another network vein in the same outcrop as 1501A sample. Shibata and Nozawa (1986) described this vein-rock as medium-grained granodiorite. On the basis of six Rb-Sr whole-rock analyses, they obtained 590-810 Ma model ages taking an initial $^{87}Sr/^{86}Sr$ ratio of 0.704. Zircon grains are euhedral, 0.14-0.27 mm in length, and 0.06-0.12 mm in width. Monazite forms euhedral to subhedral crystals of 0.09-0.18 mm in size. Most zircon grains contain less than 0.1 % UO_2, but several grains contain 0.5-1.1 % UO_2. Six analytical data from three U-rich zircon grains give an isochron (MSWD= 0.01) of 230±10 Ma with an intercept value of 0.0006±0.0006 (solid triangles, Fig. 6). Monazite grains contain 4.9-15.7 wt.% ThO_2, 0.16-0.34 wt.% UO_2 and 0.055-0.0169 wt.% PbO, and give an isochron (MSWD= 0.82) of 230±10 Ma with an intercept value of 0.0012±0.0056 (Fig. 7).

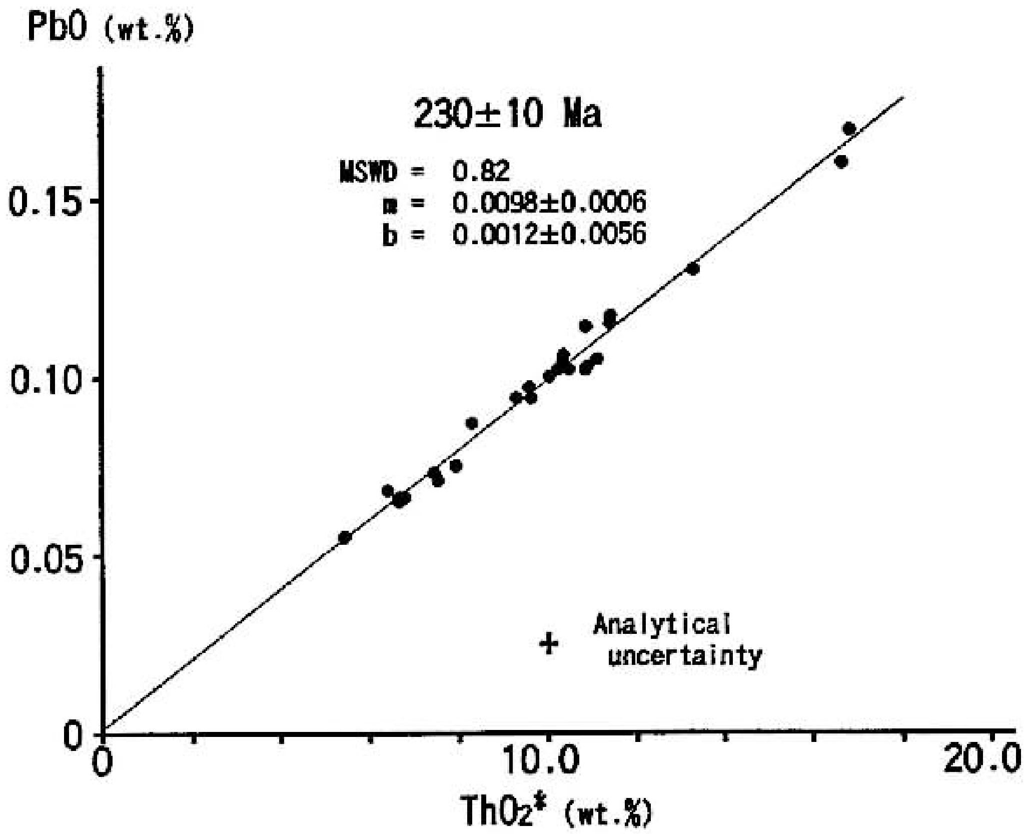

Fig. 7. Plot of PbO vs. ThO_2* for monazite grains in 1501B sample from Kagasawa. Explanation for errors is the same as for Fig. 3.

0401: Kagasawa

Zircon forms euhedral prisms with concentric growth zoning; the length hardly exceeds 0.25 mm, and the length to width ratio ranges from 1.7 to 3.3. Neither overgrowth nor outgrowth can be observed. Most zircon grains show low UO_2 and PbO contents, but 6 grains contain measurable amounts of UO_2 and PbO, 0.50-2.18 and 0.018-0.059%, respectively. The ThO_2 content ranges from 0.09 and 0.64% in cores, but rises higher than 1.1 % in rims. Data points (solid circles) for transparent portions of euhedral grains yield an isochron (MSWD= 0.38) of 250±30 Ma with an intercept value of -0.0004±0.0046 (Fig. 8). The data points (open circles) for Th-rich rims are plotted in an area below the 250 Ma isochron. Regression of these data points yields an isochron (MSWD= 0.12) of 150±30 Ma with an intercept value of 0.0047±0.0064.

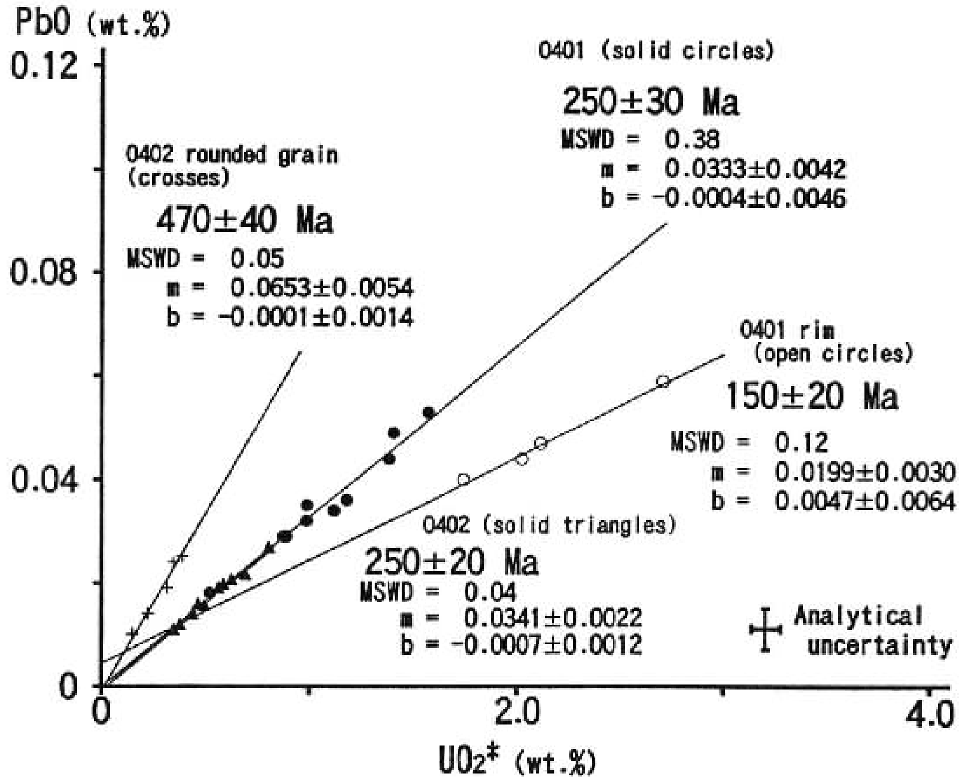

Fig. 8. Plot of PbO vs. UO_2* for zircon grains in 0401 sample from Kagasawa and 0402 sample from Man-nami. 0401: solid circles represent data points for transparent portions of euhedral grains, and open circles for Th-rich rims. 0402: solid triangles represent data points for transparent core portions of 5 euhedral grains, and crosses represent those for rounded Z05 zircon grain. Explanation for errors is the same as Fig. 3.

0402: Man-nami

Zircon grains form elongated euhedral prisms of 0.24-0.45 mm in length and 0.11-0.17 mm in width. Their UO_2 contents rise up to 0.75 % and the ThO_2/UO_2 ratios range between 0.11 and 0.57. Most data points (solid triangles) define a 250±20 Ma isochron (MSWD= 0.04) with an intercept value of -0.0007±0.0012 (Fig. 8). Data points (crosses) for Z05 rounded grain, plotted above of the 250 Ma isochron, yield an isochron of 470±40 Ma (MSWD= 0.05) with an intercept value of -0.0001±0.0014.

0403A: Man-nami River

This sample was collected from the same dike as No. 3 sample of Shibata et al. (1990). Most zircon forms euhedral prisms of 0.2-0.45 mm in length, and no rounded grain can be seen. Overgrowth texture is seen in Z11 grain where a subrounded core is mantled by a thick rim with euhedral growth zoning. The UO_2 contents range between 0.32 and 1.08 %, and the ThO_2 contents range between 0.04 and 0.43 % with two exceptionally high ThO_2 values of 2.23 and 2.43% in Z10 and Z13 grains. Most analytical data (solid circles) are arrayed linearly on the PbO-UO_2 coordinates (Fig. 9). The best-fitting isochron (MSWD= 0.19) yields an age of 240±20 Ma with an intercept value of 0.0007±0.0014. Data points (squares) for Z01 and Z07 grains and the core of Z11 core-overgrowth grain are plotted above the 240 Ma isochron. These five data points cannot regress together, but give apparent ages of 410 - 600 Ma.

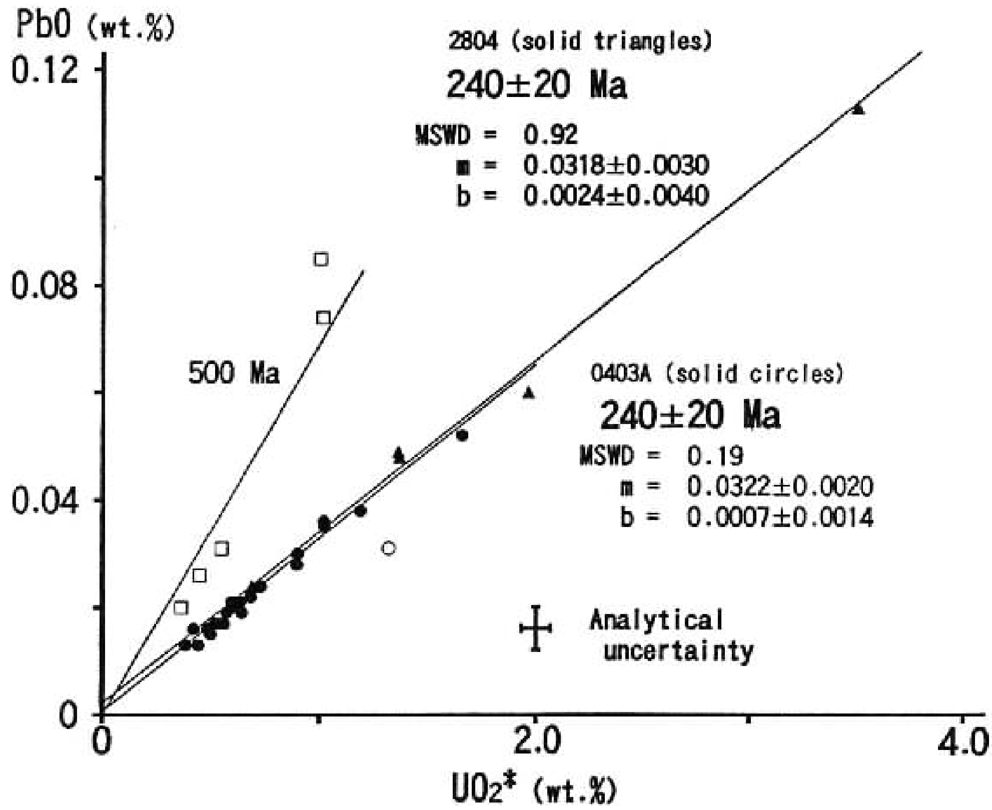

Fig. 9. Plot of PbO vs. UO_2* for zircon grains in 0403A and 2804 samples from Man-nami River. 0403A: solid circles represent data points for transparent portions of euhedral grains, open circle for Z10 grain with a high ThO_2 content, and squares data points for the rounded core of Z11 grain and for rounded Z01 and Z07 grains. 2804: microprobe analyses were carried out only for transparent portions of 6 euhedral grains (solid triangles). Explanation for errors is the same as for Fig. 3.

2804: Man-nami River

This sample was collected from the same dike as 0403A sample. Euhedral zircon grains have concentric growth zones, and their length hardly exceeds 0.2 mm. Only six grains were available for the microprobe analysis. The analytical data are plotted linearly on the PbO-UO_2 diagram (solid triangles, Fig. 9), and give an isochron (MSWD= 0.92) of 240±20 Ma with an intercept value of 0.0024±0.0040.

0403B: Man-nami River

This sample was collected from a subconcordant dike intruded into the biotite gneiss at a road cut, ca. 120 m northeast of 0403A locality. It probably corresponds to No. 2 sample of Shibata et al. (1989). Zircon occurs as euhedral prisms of 0.15-0.30 mm in length. No rounded grains can be seen in this sample, but some show abrasion at the edges. The UO_2 contents are usually less than 5 %, but some grains contain as much as 13.7 % UO_2. The ThO_2 contents range between 0.02 and 1.35 %. Although data points for rims and metamict portions (open circles) are highly scattered, those for clear portions (solid circles) are arrayed linearly on the PbO-UO_2^* diagram (Fig. 10). The best-fitting isochron (MSWD= 0.44) gives an age of 240±10 Ma and an intercept value of 0.0009±0.0019. The Z10 grain with abraded edges (square) gives an apparent age of 670 Ma.

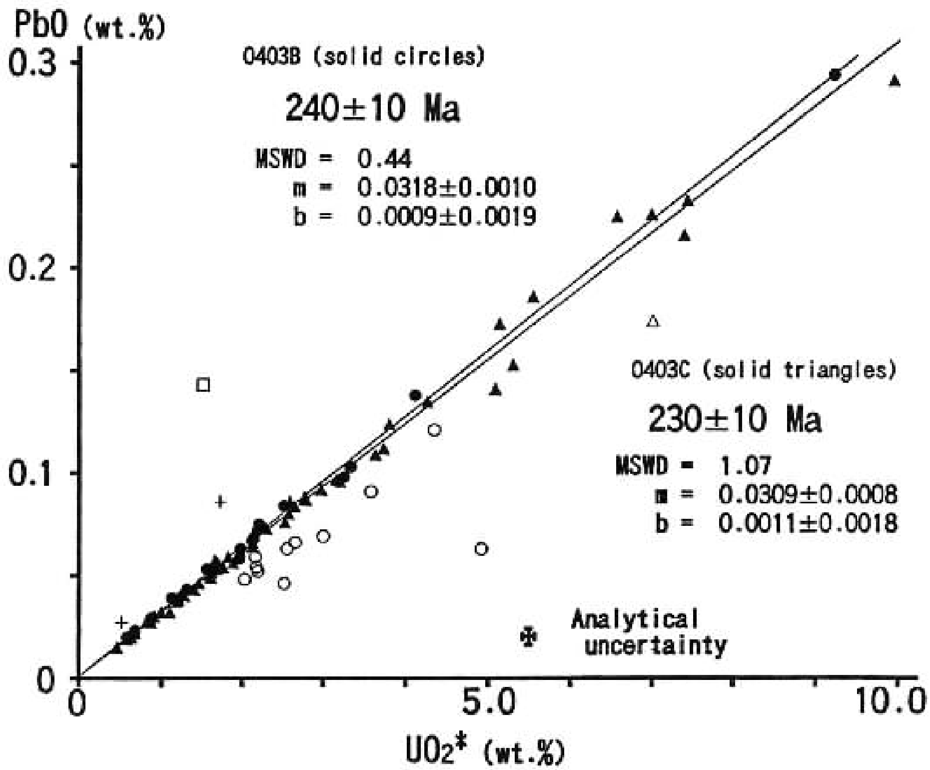

Fig. 10. Plot of PbO vs. UO_2^* for zircon grains in 0403B and 0403C samples from Man-nami River. 0403B: solid circles represent data points for transparent portions of euhedral grains, open circles for rims and metamict portions, and square subrounded Z10 grain. 0403C: solid triangles represent data points for transparent and translucent portions of euhedral grains, open triangle for a metamict rim, and crosses for the subrounded core of Z09 core-overgrowth grain. Explanation for errors is the same as for Fig. 3.

0403C: Man-nami River

This sample, collected from the central part of a ca. 1 m thick dike in the biotite gneiss, probably corresponds to No. 10 sample of Shibata et al. (1989). Zircons form euhedral prisms of 0.18 - 0.31 mm in length, and their length to width ratios range between 2.0 and 3.3. Most grains are well faceted and show concentric growth zones. Overgrowth is seen only in one grain (No. Z09), where a clear subrounded core is mantled by translucent rim with concentric growth zoning. Turbidity in the zircon is variable from portion to portion within a single grain. The UO_2 contents range from 0.57 to 24.6 %, and the ThO_2 contents from 0.01 to 2.58 %. Analytical data (triangles) are plotted within a narrow band passing through the origin (Fig. 10). Data points for rims and highly metamict portions are plotted outside of the area shown in Fig. 10, and tend to shift toward the lower side within the band. Two data points plotted above the band (crosses) are those for the rounded core of Z09 grain. All data listed in Appendix 2 define an isochron (MSWD= 2.52) of 220±10 Ma. If the data points (solid triangles on Fig. 10) for transparent and translucent portions regress together, the MSWD decreases to 1.07 and the isochron age is 230±10 Ma with an intercept value of 0.0011±0.0018.

2801B: Amo

Zircon forms well-faceted crystals of 0.2-0.4 mm in length. They have high length to width ratios between 2.8 and 6.9. The UO_2 contents rise up to 5.35 % and the ThO_2 contents up to 6.90 %. The ThO_2/UO_2 ratios, ranging between 0.063 and 1.48, average 0.75. Most data points (solid circles, 28 of 29 analyses on 17 zircon grains) are arrayed

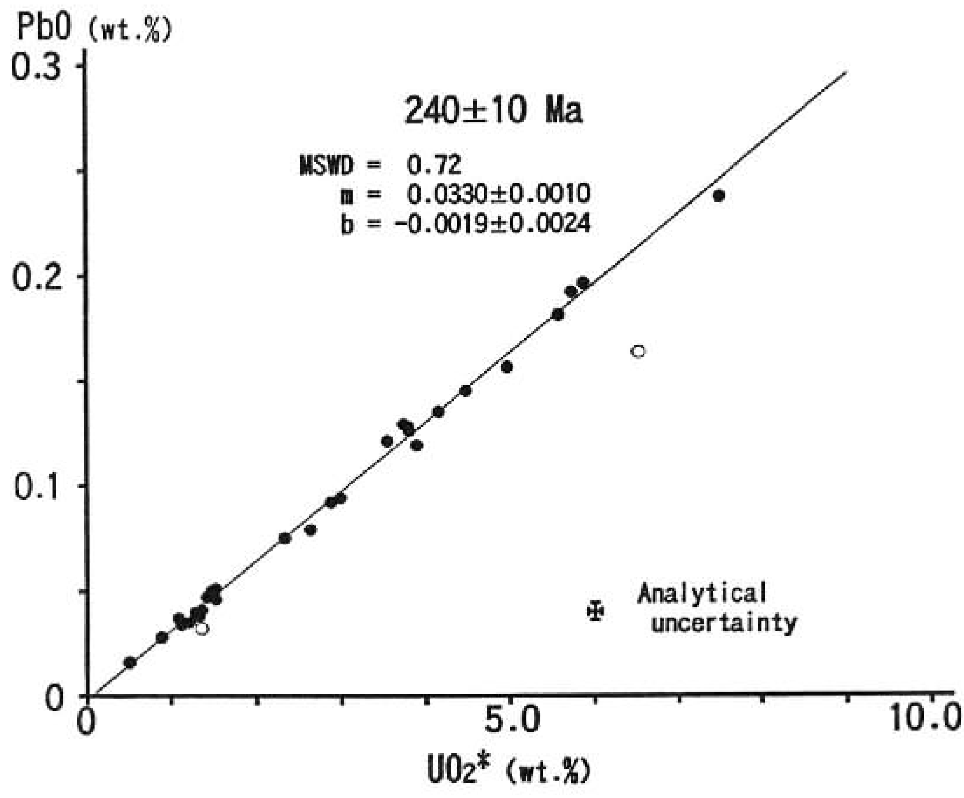

Fig. 11. Plot of PbO vs. UO_2* for zircon grains in 2801B sample from Amo. Solid circles represent data points for transparent and translucent portions of euhedral grains, and open circles represent highly metamict spot 3 of Z01 and spot Z of 210 grains. Explanation as for Fig. 3.

linearly (Fig. 11), and yield an isochron of 240±10 Ma with an intercept value of -0.0019±0.0024.

DISCUSSION

The chemical Th-U-total Pb isochron ages of euhedral zircon grains and monazite grains concentrate at about 240 Ma. Ages as old as 1270 Ma are obtained only in the rounded zircon grains and the rounded cores of core-overgrowth grains. Although the 240 Ma CHIME age for zircon and monazite coincides well with the age of main metamorphism in the Hida terrane (Ishizaka and Yamaguchi, 1969; Shibata et al., 1970), it is significantly younger than the Rb-Sr whole-rock isochron age of 506±37 Ma for the Gray Granite (Shibata et al., 1989). This discrepancy between the CHIME age and the isotopic age cannot be ascribed to error in the microprobe analysis. It might be thought that the 240 Ma age could result from the combined effects of partial Pb loss from restricted portions of single grains and a heterogeneous distribution of the initial Pb. These effects, if present, would displace the isochron significantly below or above the origin of the PbO-UO_2* (ThO_2*) diagram. Since the isochrons pass through the origin, such possibilities are excluded.

Some may consider that the Gray Granite originated 506 Ma ago and underwent total recrystallization and/or rejuvenescence through a significant thermal event at 240 Ma. Most 240 Ma zircons, however, show concentric growth zones attributable to crystallization from viscous felsic melts (Speer, 1980). The intra-grain distributions of Th and U coincide well with the growth zones. These suggest that ta otal loss of Pb from zircon through the ca. 240 Ma thermal event is unlikely. Furthermore, the concordant PbO-UO_2* relations (dated back to 1270 Ma) within some rounded cores of core-overgrowth crystals do not favor the possibility.

To obtain a better understanding of the cause for the discrepancy between the CHIME and isotopic ages, we examined the distribution of Sr and Rb in the Gray Granite. Figure 12 illustrates X-ray emission spectra around SrLα and RbLα for constituent minerals in 0403-A sample. The figure clearly shows that Sr is concentrated in K-feldspar, plagioclase, allanite and apatite; the Sr content of K-feldspar amounts to 440-680 ppm, plagioclase 740-1050 ppm, allanite 910-1720 ppm, and apatite about 130 ppm. The Sr contents of biotite, muscovite, epidote and titanite are in less than the 2σ detection limit (ca. 40 ppm). On the other hand, Rb concentrates mainly in biotite, K-feldspar and muscovite; the Rb content of biotite is in the range between 220-890 ppm with a maximum value of 1040 ppm on a least altered portion, K-feldspar 340-370 ppm and muscovite about 420-470 ppm. The Rb content of plagioclase is less than 80 ppm. Figure 13 illustrates a line profile of SrLα intensity across constituent minerals in H7 sample of Shibata et al. (1989). The SrLα intensity rises extraordinarily on some sericitized portions of plagioclase and some grain-boundaries. The maximum count rate on sericitized portions of plagioclase is 2190 ppm Sr, and that on grain-boundaries 2570 ppm Sr. The sericitized portions of plagioclase showing 2190 ppm Sr contain 290 ppm Rb, and the grain-boundaries with 2570 ppm Sr contain only 70 ppm Rb. Some large

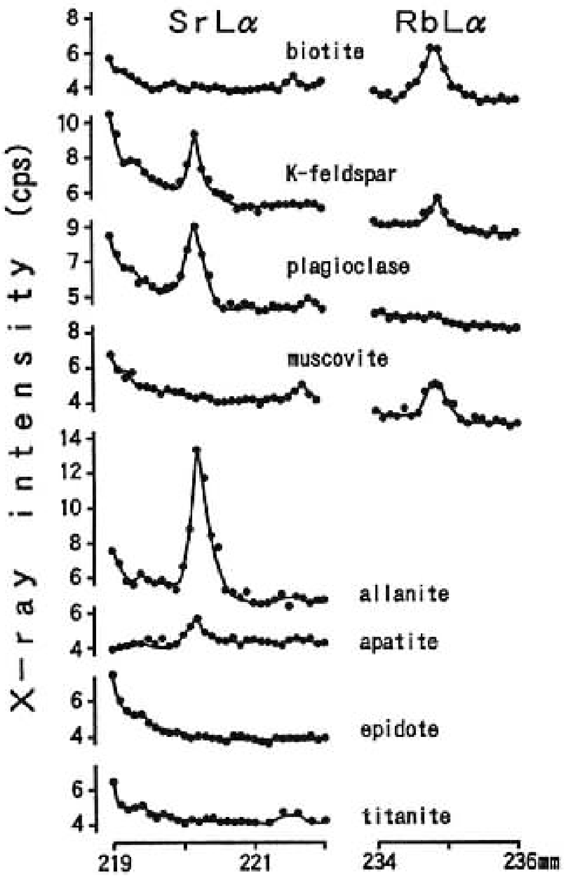

Fig. 12. X-ray spectra in the SrLα and RbLα regions for biotite, K-feldspar, plagioclase, muscovite, allanite, apatite, epidote and titanite in 0403A sample. The ordinates represent X-ray intensity (cps) and the scales of abscissas represent the X-ray detection position (mm) of the JEOL spectrometer. The rise in count toward 219 mm represents the low-energy envelope of SiKβ band. The high background intensity in the SrLα spectra of K-feldspar and plagioclase comes from the high concentration of SiO_2.

flakes (0.02 - 0.04 mm long) of secondary sericite in plagioclase contain 110 - 180 ppm Rb.

Since biotite has been mostly chloritized in entire samples of the Gray Granite, Rb in biotite, probably a significant portion of the whole-rock Rb, has been lost through the alteration process. Sericitization of plagioclase is also a common feature in the Gray Granite. Apart from the question of what phase has concentrated Sr, these altered portions apparently gained a certain amount of Sr. The microprobe examination shows that the Gray Granite was open with respect to Rb and Sr during the alteration. As noted previously, the whole-rock Rb-Sr isotopic data presented by Shibata et al. (1989) are highly scattered. This may result, at least in part, from the heterogeneous disturbance of Rb and Sr, as recognized here. Presumably the 506 Ma Rb-Sr whole-rock isochron age does not represent any significant episode. Instead, it seems much more likely that the

Gray Granite was emplaced about 240 Ma ago with new growth of zircons. Furthermore, the zircon and monazite ages of ca. 240 Ma correspond well with the 231±11 Ma K-Ar hornblende age determined on a Gray Granite sample from Amo (Ota and Itaya, unpublished data appeared in Ota and Itaya, 1989).

Some of the Gray Granite contains rounded zircon both as discrete grains and cores of core-overgrowth grains. Because these rounded grains give varying CHIME ages from 340 to 1270 Ma, they should be of inherited origin. The presence of such inherited zircon grains indicates that recycled older materials contributed to the generation and/or evolution of the Gray Granite magma(s). The contribution of recycled materials also accounts for the significant intra-sample scatter of whole-rock Rb-Sr data for the Gray Granite. It seems, then, that the Precambrian Rb-Sr whole-rock model ages reported by Sato et al. (1967) and Shibata and Nozawa (1986) come probably from a higher proportion of the recycled Precambrian materials, such as the 1493 Ma rounded zircon population (Ishizaka and Yamaguchi, 1969). Obviously these Precambrian detritus cannot be considered indicative of the Precambrian origin of the Hida gneiss.

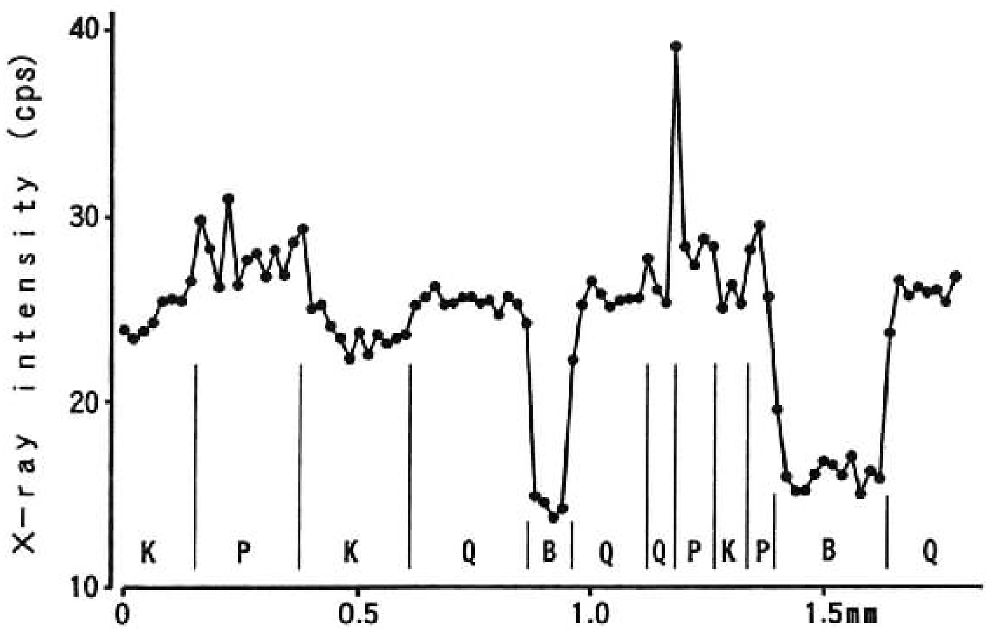

Fig. 13. Line profile of X-ray intensity (SrLα) across constituent minerals (K: K-feldspar, P: plagioclase, Q: quartz, B: biotite) in H7 sample of Shibata et al. (1989). The X-ray intensity includes the SrLα characteristic line, interferences from SiKβ and backgrounds. The count rate rises on the sericitized portion of plagioclase at left and the grain-boundaries between quartz grains and between quartz and plagioclase grains at central right.

CONCLUDING REMARKS

The chemical Th-U-total Pb isochron ages of zircon and monazite have revealed that the Gray Granite originated in Triassic time (ca. 240 Ma), but evidently not in

Precambrian time. Since the Gray Granite was open with respect to Rb and Sr during chloritization of biotite and sericitization of plagioclase, the Rb-Sr whole-rock isochron age of 506 Ma by Shibata et al. (1989) is incorrect. Consequently, the previous view that the Gray Granite is of Precambrian origin and that the Hida gneisses cut by the Gray Granite were therefore formed in Precambrian time, is no longer valid. Age determinations of zircon and monazite from the Hida gneisses are essential to a correct understanding of the origin and development of the Hida gneiss complex.

ACKNOWLEDGEMENTS

We thank Drs Y. Tsuzuki and T. Tanaka for their helpful discussion, Dr. H. Shimizu for his careful review, and Mr. K. Ota for providing samples 2801B and 2804. This work was supported in part by a Grant- in-Aid for Fundamental Scientific Research (Nos. 63460053 and 03452068) from the Ministry of Education, Science and Culture, Japan.

REFERENCES

AMLI, R. and W. GRIFFIN (1975) Microprobe analysis of REE minerals using empirical correction factors. Am. Mineral., vol. **60**, 599 - 606.

DRAKE, M.J. and D.F. WEILL (1972) New rare earth element standards for electron microprobe analysis. Chem. Geol., vol. **10**, 179 - 181.

HIROI, Y., N. FUJI and Y. OKIMURA (1978) New fossil discovery from the Hida metamorphic rocks in the Unazuki area, central Japan. Proc. Japan Acad., vol. **64**, B, 268 - 271.

ICHIKAWA, K (1990) Pre-Cretaceous terranes of Japan. In *Pre-Cretaceous terranes of Japan*, edited by K. Ichikawa, S.Mizutani, I. Hara, S. Hada and A. Yao, Publication of IGCP Project 224, 1 - 11.

ISHIZAKA, K. and M. YAMAGUCHI (1969) U-Th-Pb ages of sphene and zircon from the Hida metamorphic terrain, Japan. Earth Planet. Sci. Lett., vol. **6**, 179 - 185.

KANO, T. (1982) Tectonic divisions and their development of the Hida metamorphic region, central Japan. Mem. Geol. Soc. Japan, No. **21**, 9 - 24.

OTA, K. and T. ITAYA (1989) Radiometric ages of granitic and metamorphic rocks in the Hida metamorphic belt, central Japan. Bull. Hiruzen Res. Inst., Okayama University of Science, No. 15, 1 - 25.

SATO, S. (1968) Precambrian - Variscan polymetamorphism in the Hida massif, basement of the Japanese Islands. Sci. Rept. Tokyo Univ. Educ., Sec. C, vol. **10**, 15 - 129.

SATO, S., T. SHIRAHASE and H. SHIBATA (1967) Older granite based on the Rb-Sr dating in the Hida massif. Jour. Geol. Soc. Japan, vol. **73**, 72.

SHIBATA, K., T. KANO and M. ASANO (1989) Isotopic ages of the Gray granite from the upper Kubusu River area, Hida Mountains. Jour. Min. Pet. Econ. Geol., vol. **84**, 243 - 251.

SHIBATA, K. and T. NOZAWA (1984) Isotopic ages of the Funatsu Granitic Rocks. Jour. Japan Assoc. Min. Pet. Econ. Geol., vol. **79**, 289 - 298.

SHIBATA, K. and T. NOZAWA (1986) Late Precambrian ages for granitic rocks intruding the Hida Metamorphic Rocks. Bull. Geol. Surv. Japan, vol. **36**, 43 - 51.

SHIBATA, K., T. NOZAWA and R.K. WANLESS (1970) Rb-Sr geochronology of the Hida metamorphic belt, Japan. Can. Jour. Earth Sic., vol. **7**, 1383 - 1401.

SMELLIE, J.A.T., N. COGGER and J. HERRINGTON (1978) Standards for quantitative microprobe determination of uranium and thorium with additional information on the chemical formulae of davidite and euxenite-polycrase. Chem. Geol., vol. **22**, 1 - 10.

SPEER, J.A. (1980) Zircon. In: *Orthosilicates* (Review in Mineralogy 5), edited by P.H. Ribbe, Mineralogical Society of America, 67 - 112.

STEIGER, R.H. and E. JÄGER (1977) Subcommission on geochronology: convention on the use of decay constants in geo- and cosmochronology. Earth Planet. Sci. Lett., vol. **36**, 359 - 362.

SUWA, K. (1969) Polymetamorphism in the Hida metamorphic complex. Mem. Geol. Soc. Japan,, No. 4 113 - 116.

SUWA, K. (1990) Hida-Oki terrane. In: *Pre-Cretaceous terranes of Japan*, edited by K. Ichikawa, S. Mizutani, I. Hara, S. Hada and A. Yao, Publication of IGCP Project 224, 13 - 24.

SUZUKI, K. and M. ADACHI (1991) Precambrian provenance and Silurian metamorphism of the Tsubonosawa paragneiss in the South Kitakami terrane, Northeast Japan, revealed by the Th-U-total Pb chemical isochron ages of monazite, zircon and xenotime. Geochemical J., vol. 25, 357 - 376.

SUZUKI, K., M. ADACHI and T. TANAKA (1991) Middle Precambrian provenance of Jurassic sandstone in the Mino terrane, central Japan: evidence from an electron microprobe Th-U-total Pb monazite study. Sediment. Geol., vol. **75**, 141 - 147.

SUZUKI, M. (1977) Polymetamorphism in the Hida Metamorphic Belt, central Japan. Jour. Sci. Hiroshima Univ., vol. **7**, 217 - 296.

YORK, D. (1966) Least-squares fitting of a straight line. Can. J. Phy., vol. **44**, 1079 - 1088.

Appendix 1: Outline of the chemical Th-U-total Pb isochron method (CHIME).

Zircon and monazite contain both U and Th. Natural Th consists of only a radioactive isotope of ^{232}Th, and natural U consists of two radioactive isotopes, ^{235}U and ^{238}U. These radioactive isotopes decay into Pb:

$$^{232}Th \longrightarrow 6 \text{ alphas} + 4 \text{ betas} + {}^{208}Pb \quad (a)$$
$$^{235}U \longrightarrow 7 \text{ alphas} + 4 \text{ betas} + {}^{207}Pb \quad (b)$$
$$^{238}U \longrightarrow 8 \text{ alphas} + 6 \text{ betas} + {}^{206}Pb \quad (c)$$

The number of atoms of ^{208}Pb, ^{207}Pb and ^{206}Pb which accumulate in a time τ is given in terms of the present-day amounts of ^{232}Th, ^{235}U and ^{238}U;

$$^{208}Pb = {}^{232}Th\ \{\exp(\lambda_{232}\tau) - 1\} \quad (d)$$
$$^{207}Pb = {}^{235}U\ \{\exp(\lambda_{235}\tau) - 1\} \quad (e)$$
$$^{206}Pb = {}^{238}U\ \{\exp(\lambda_{238}\tau) - 1\} \quad (f)$$

where λ symbolizes the decay constant of each isotope; $\lambda_{232}= 4.9475\text{x}10^{-11}/\text{y}$, $\lambda_{235}= 9.8485\text{x}10^{-10}/\text{y}$ and $\lambda_{238}=1.55125\text{x}10^{-10}/\text{y}$ (Steiger and Jäger, 1977).

Uranium- and Thorium-bearing zircon and monazite contain initial (common) Pb as well as radiogenic one

$$\begin{aligned}\text{Total Pb} &= Pb_{initial} + {}^{208}Pb + {}^{207}Pb + {}^{206}Pb \\ &= Pb_{initial} + {}^{232}Th\{\exp(\lambda_{232}\tau) - 1\} \\ &\quad + {}^{235}U\{\exp(\lambda_{235}\tau) - 1\} \\ &\quad + {}^{238}U\{\exp(\lambda_{238}\tau) - 1\} \qquad (g)\end{aligned}$$

Since the $^{235}U/^{238}U$ ratio is 137.88 (Steiger and Jäger, 1977), Eq. (g) can be written:

$$\begin{aligned}\text{Total Pb} &= Pb_{initial} \\ &\quad + {}^{232}Th\ \{\exp(\lambda_{232}\tau) - 1\} \\ &\quad + U\left\{\frac{137.88\exp(\lambda_{238}\tau) + \exp(\lambda_{235}\tau)}{138.88} - 1\right\} \qquad (h)\end{aligned}$$

The chemical Th-U-total Pb isochron method (CHIME; Suzuki et al. 1991; Suzuki and Adachi, 1991) is as follows. We obtain, in the first step, an apparent age (t) from each set of the UO_2, ThO_2 and PbO concentrations (wt.%) by solving the equation;

$$\begin{aligned}\frac{PbO}{W_{Pb}} &= \frac{ThO_2}{W_{Th}}\{\exp(l_{232}t) - 1\} \\ &\quad + \frac{UO_2}{W_U}\left\{\frac{\exp(\lambda_{235}t) + 138\exp(\lambda_{238}t)}{139} - 1\right\} \qquad (l)\end{aligned}$$

where W symbolizes the gram-molecular weight of each oxide. We assume W_{Pb}= 222 (206+16) for U-rich zircon, W_{Pb}=224 (208+16) for Th-rich monazite, W_{Th}=264 (232+32), W_U=270 (238+32) and $^{238}UO_2/^{235}UO_2$=138. Taking the apparent age (t), we turn the sum of ThO_2 and UO_2 into ThO_2^* (monazite) or UO_2^* (zircon) by:

$$ThO_2^* = ThO_2 + \frac{UO_2 \cdot W_{Th}}{W_U\{\exp(\lambda_{232}t) - 1\}}\left\{\frac{\exp(\lambda_{235}t) + 138\exp(\lambda_{238}t)}{139} - 1\right\} \tag{2}$$

$$UO_2^* = UO_2 + \frac{139\, ThO_2 \cdot W_U\{\exp(\lambda_{232}t) - 1\}}{W_{Th}\{\exp(\lambda_{235}t) + 138\exp(\lambda_{238}t) - 139\}} \tag{2'}$$

If cogenetic mineral grains and/or individual parts of a single mineral grain contain the same amounts of initial Pb but different amounts of Th and U, and have remained in a closed system, all analytical data will be plotted on a straight line with the slope (m) and intercept (b),

$$PbO = m \cdot ThO_2^* + b \quad \text{(monazite)} \tag{3}$$

$$PbO = m \cdot UO_2^* + b \quad \text{(zircon)} \tag{3'}$$

We determine the best-fitting regression line through the procedure proposed by York (1966), taking account of uncertainties in the microprobe analyses, and calculate the first approximation of age (T) from the slope (m) of equations:

$$T = \frac{1}{\lambda_{232}} \ln\left(1 + m\frac{W_{Th}}{W_{Pb}}\right) \quad \text{(monazite)} \tag{4}$$

$$m\frac{W_U}{W_{Pb}} = \frac{\exp(\lambda_{235}T) + 138\exp(\lambda_{238}T)}{139} - 1 \quad \text{(zircon)} \tag{4'}$$

Then, we can obtain the second approximation by replacing the apparent ages (t) of equation (2 or 2') with the first approximation age (T), and so on. The intercept (b) of the line is assumed to represent the concentration (wt.%) of the initial PbO. Normally, a significant amount of initial Pb or Pb-loss, if any, would deviate the line from the origin, or would not form an isochron.

Appendix 2: Analytical data of zircon (Z), monazite (M), allanite (A) and thorite (T). nd: not detected, C: core of core-overgrowth grain, M: mantle of core-overgrowth grain, R: rim, r: rounded grain, m: metamict grain, UO_2*: sum of measured UO_2 and UO_2 equivalent of measured ThO_2 for zircon, and ThO_2*: sum of measured ThO_2 and ThO_2 equivalent of measured UO_2 for others.

Sample & Grain No.	ThO_2 (wt%)	UO_2 (wt%)	PbO (wt%)	t (Ma)	UO_2* ThO_2*
(No. 0701A)					
Z03	0.011	0.043	nd	-	-
Z04-01	0.038	0.281	0.010	250	0.293
Z04-02	0.260	0.476	0.018	240	0.556
Z04-03	0.164	0.312	0.012	240	0.363
Z04-04	0.039	0.291	0.010	240	0.303
Z07-01	1.44	0.847	0.044	250	1.29
Z07-02	0.768	0.587	0.027	240	0.824
Z07-03	0.089	0.149	nd	-	-
Z07-04 R	1.25	0.679	0.028	190	1.07
Z08	0.073	0.168	nd	-	-
Z09-01 R	2.41	0.738	0.036	180	1.49
Z09-02	0.178	0.196	nd	-	-
Z12	1.17	0.984	0.044	240	1.35
Z13-01	0.341	0.339	0.014	230	0.444
Z13-02	0.345	0.305	0.014	250	0.411
Z13-03	0.280	0.283	0.013	260	0.369
Z14-01	0.169	0.177	nd	-	-
Z14-02	0.237	0.629	0.025	260	0.702
Z14-03	0.793	0.473	0.021	220	0.718
(No. 0701B)					
Z06	nd	0.040	nd	-	-
Z07-01	0.723	0.761	0.032	240	0.984
Z07-02	0.255	0.445	0.017	240	0.524
Z07-03	0.251	0.419	0.017	250	0.496
Z08	nd	0.039	nd	-	-
Z10-01	0.924	1.04	0.045	250	1.32
Z10-02	0.280	0.459	0.017	230	0.545
Z10-03	0.704	0.939	0.041	260	1.16
Z11-01	0.353	0.536	0.023	260	0.645
Z11-02	0.685	0.784	0.032	240	0.995
Z14	0.280	0.536	0.023	270	0.622
A15	10.9	0.246	0.090	180	11.7
Z16	0.248	0.680	0.024	230	0.757
Z17	0.197	0.313	0.013	260	0.374
Z18	0.143	0.196	nd	-	-
Z19	0.522	0.779	0.021	170	0.941
Z20	0.623	0.689	0.027	230	0.881
Z21	0.240	0.413	0.016	240	0.487
Z22 r	0.017	0.153	0.013	590	0.158
Z23	0.190	0.399	0.014	230	0.458
Z24	0.180	0.324	0.013	250	0.380
Z25	0.562	0.685	0.027	230	0.859
Z26	0.186	0.478	0.018	250	0.535
Z27-01	0.220	0.579	0.022	250	0.647
Z27-02	0.184	0.418	0.014	220	0.475
Z28	0.364	0.368	0.015	230	0.480
Z29-01	0.846	0.845	0.034	230	1.11
Z29-02 R	0.644	0.653	0.021	180	0.853
Z30	0.376	0.790	0.030	240	0.906
Z31-01 R	0.531	0.793	0.025	190	0.958
Z31-02	0.265	0.381	0.017	270	0.463
Z32	0.133	0.252	0.009	230	0.293
Z33	0.298	0.510	0.019	230	0.602
Z34-01	0.446	0.557	0.023	240	0.695
Z34-02	0.371	0.547	0.022	250	0.661
Z35	0.044	0.089	nd	-	-
Z36	0.215	0.347	0.013	230	0.413
Z37	0.024	0.041	nd	-	-
A38	10.9	0.246	0.090	180	11.7

Appendix 2 (cont'd)

Sample & Grain No.	ThO_2 (wt%)	UO_2 (wt%)	PbO (wt%)	t (Ma)	UO_2* ThO_2*
(No. 0702A)					
Z01-01	5.77	2.44	0.136	240	4.22
Z01-02	1.31	1.09	0.046	230	1.49
Z03-01	0.242	0.542	0.020	240	0.617
Z03-02	2.98	0.963	0.047	180	1.89
Z04	0.386	0.463	0.017	220	0.582
Z05	0.155	0.248	0.010	250	0.296
Z06	0.347	0.330	0.014	240	0.437
Z07	0.429	0.550	0.022	240	0.682
Z08	0.418	0.433	0.019	250	0.562
Z09-01	0.333	0.601	0.024	250	0.704
Z09-02	0.846	1.35	0.052	240	1.61
Z10-01	0.255	0.576	0.022	250	0.655
Z10-02	0.084	0.725	0.024	240	0.751
Z11-01	2.81	1.20	0.071	250	2.07
Z11-02	1.90	1.33	0.064	250	1.92
Z12	2.19	1.24	0.051	200	1.92
Z15	0.955	0.751	0.034	240	1.05
Z16	2.28	1.64	0.052	160	2.35
Z17	1.85	1.37	0.096	360	1.94
Z18	0.500	1.14	0.042	240	1.29
(No. 07002B)					
Z01	0.020	0.039	nd	-	-
Z03-01 C	1.53	1.25	0.303	1190	1.69
Z03-02 C	0.669	0.709	0.157	1160	0.900
Z03-03 C	1.25	1.09	0.261	1200	1.45
Z03-04 C	0.735	0.710	0.161	1170	0.920
Z03-05 C	1.53	1.13	0.289	1230	1.57
Z03-06 C	1.81	1.28	0.312	1160	1.80
Z03-07 M	0.168	0.376	0.015	260	0.428
Z04-01	0.113	0.425	0.014	220	0.460
Z04-02	0.084	0.378	0.015	270	0.404
Z04-03	0.112	0.408	0.014	230	0.443
Z04-04	0.050	0.262	0.010	270	0.277
Z04-05 R	0.104	0.420	0.011	180	0.452

Sample & Grain No.	ThO_2 (wt%)	UO_2 (wt%)	PbO (wt%)	t (Ma)	UO_2* ThO_2*
Z05-01 M	0.643	0.825	0.035	250	1.02
Z05-02 M	1.75	1.29	0.053	210	1.83
Z05-03 C	1.03	1.55	0.091	360	1.87
Z05-04 C	1.08	1.13	0.100	500	1.46
Z05-05 C	1.87	2.35	0.136	340	2.92
Z05-06 C	0.511	0.537	0.040	420	0.693
Z05-07 C	1.05	0.825	0.073	460	1.14
Z05-08 C	1.59	1.71	0.127	420	2.19
Z05-09 C	1.46	1.49	0.086	320	1.94
Z05-10 C	1.64	1.38	0.177	670	1.87
Z05-11 C	0.669	0.816	0.075	530	1.02
Z05-12 C	1.50	1.69	0.160	530	2.14
Z08 R	1.16	1.67	0.051	190	2.03
Z09-01 r	1.46	1.37	0.082	330	1.82
Z09-02 r	2.83	1.80	0.133	360	2.67
Z10	0.145	0.267	0.010	240	0.312
Z11	0.860	1.06	0.043	240	1.33
T12-01	68.7	7.10	0.271	70	91.4
T12-02	68.4	9.40	0.277	70	98.5
Z14-01 C	1.51	1.26	0.079	330	1.72
Z14-02 C	0.512	0.750	0.041	330	0.907
Z14-03 C	0.454	0.582	0.035	350	0.721
Z14-04 C	1.45	1.96	0.111	340	2.40
Z14-05 C	0.464	0.916	0.048	330	1.06
Z14-06 M	0.580	1.28	0.056	280	1.46
Z14-07 M	0.703	0.847	0.031	220	1.06
Z14-08 M	0.222	0.447	0.015	220	0.516
Z14-09 M	0.216	0.459	0.017	240	0.526
Z14-10 M	0.408	0.778	0.029	240	0.904
Z14-11 M	0.084	0.249	0.009	240	0.275
Z14-12 R	0.111	0.303	0.008	180	0.337
Z14-13 R	0.106	0.333	0.009	180	0.366
Z14-14 M	0.013	0.375	0.012	230	0.379
Z14-15 R	0.426	0.482	0.017	200	0.614
Z14-16 M	0.899	2.11	0.083	260	2.39
Z14-17 M	0.132	0.245	0.010	260	0.286
Z14-18 M	0.733	1.33	0.056	270	1.56
Z14-19 M	2.52	1.24	0.057	210	2.02
Z15-01 r	0.172	0.446	0.024	350	0.499

Appendix 2 (cont'd)

Sample & Grain No.	ThO_2 (wt%)	UO_2 (wt%)	PbO (wt%)	t (Ma)	UO_2* ThO_2*
Z15-02 r	0.173	0.268	0.015	340	0.321
Z16-01 C	1.34	1.84	0.152	490	2.25
Z16-02 C	1.46	1.62	0.138	480	2.06
Z16-03 C	1.50	1.68	0.140	470	2.13
Z16-04 C	2.49	2.95	0.268	520	3.70
Z16-05 C	1.85	2.73	0.214	470	3.29
Z16-06 C	2.08	2.30	0.205	500	2.93
Z16-07 C	2.17	1.89	0.159	450	2.55
Z16-08 C	0.484	0.819	0.064	480	0.966
Z16-09 M	0.173	0.462	0.018	260	0.515
Z16-10 M	0.092	0.251	0.010	260	0.279
Z16-11 M	0.177	0.483	0.018	250	0.538
Z16-12 M	0.171	0.471	0.017	240	0.524
Z16-13 M	0.269	0.588	0.023	250	0.671
Z17	0.998	0.773	0.034	230	1.08
Z20-01	0.035	0.433	0.015	250	0.444
Z20-02 R	0.933	1.62	0.045	170	1.91
Z21-01	0.370	0.335	0.015	250	0.449
Z21-02	0.179	0.424	0.016	250	0.479
Z21-03	0.186	0.366	0.013	230	0.423
Z22	0.193	0.362	0.013	230	0.422
Z23	0.136	0.315	0.011	230	0.357
Z24	0.426	0.770	0.026	210	0.902
(No. 15001A)					
Z01	0.018	0.236	nd	-	-
Z02-01	0.116	0.566	0.019	230	0.602
Z02-02	0.196	0.785	0.026	230	0.846
Z02-03	0.126	0.614	0.024	270	0.653
Z03-01	0.119	0.494	0.020	280	0.531
Z03-02	0.062	0.345	0.013	260	0.364
Z04	0.116	0.489	0.017	240	0.525
Z05-01	0.427	1.40	0.050	240	1.53
Z05-02	0.397	1.31	0.051	260	1.43
Z05-03	0.083	0.425	0.016	260	0.451
Z05-04	0.478	1.26	0.047	250	1.41

Sample & Grain No.	ThO_2 (wt%)	UO_2 (wt%)	PbO (wt%)	t (Ma)	UO_2* ThO_2*
Z06	0.073	0.455	0.016	250	0.478
Z07	0.118	0.459	0.017	250	0.495
Z08-01	0.273	0.772	0.030	260	0.856
Z08-02	0.229	0.719	0.026	240	0.790
Z08-03	0.222	0.670	0.024	240	0.739
Z08-04	0.208	0.639	0.026	270	0.703
Z09	0.067	0.491	0.018	260	0.512
Z10	0.072	0.348	0.012	240	0.370
Z11-01	1.30	1.87	0.072	230	2.27
Z11-02	0.291	0.790	0.027	230	0.880
Z11-03 R	4.81	2.90	0.098	170	4.39
Z11-04	1.27	1.77	0.073	250	2.16
Z11-05	0.358	0.655	0.026	250	0.765
Z12-01	0.209	0.974	0.034	240	1.04
Z12-02	0.183	0.876	0.030	240	0.932
Z12-03 R	0.269	1.29	0.032	170	1.37
Z13	0.083	0.328	0.011	230	0.354
Z14	0.140	0.493	0.018	250	0.536
Z15	0.107	0.398	0.015	260	0.431
Z16-01	1.96	5.24	0.192	240	5.84
Z16-02 R	0.306	1.73	0.047	190	1.82
Z16-03	0.053	0.425	0.015	250	0.441
Z16-04	0.236	1.42	0.045	220	1.49
Z16-05	0.281	1.15	0.044	260	1.24
Z16-06	1.05	2.05	0.082	250	2.37
Z16-07	0.576	1.34	0.052	250	1.52
Z16-08	0.064	0.464	0.016	240	0.484
Z16-09	0.064	0.692	0.023	240	0.712
Z17	0.114	0.516	0.020	270	0.551
Z18-01	0.532	1.28	0.049	250	1.44
Z18-02	0.193	0.528	0.019	240	0.588
Z18-03	0.590	1.38	0.050	240	1.56
Z19-01	0.608	0.710	0.031	250	0.898
Z19-02	0.168	0.545	0.020	250	0.597
Z19-03	0.197	0.692	0.024	240	0.753
Z19-04	0.387	1.02	0.039	250	1.14
Z19-05	1.40	2.17	0.086	240	2.60
Z19-06	0.565	1.21	0.045	240	1.38

Appendix 2 (cont'd)

Sample & Grain No.	ThO_2 (wt%)	UO_2 (wt%)	PbO (wt%)	t (Ma)	UO_2^* ThO_2^*
(No. 15001B)					
Z01-01	0.109	0.507	0.018	250	0.541
Z01-02	0.220	0.962	0.033	240	1.03
Z02-01	0.070	0.406	0.014	240	0.428
Z02-02	0.323	1.12	0.039	240	1.22
Z02-03	0.138	0.573	0.020	240	0.616
Z03	0.023	0.491	0.016	240	0.498
Z04	0.029	0.081	nd	-	-
M01-01	10.3	0.334	0.115	240	11.4
M01-02	10.5	0.284	0.117	240	11.4
M01-03	8.42	0.268	0.094	240	9.29
M01-04	9.97	0.289	0.103	220	10.9
M01-05	9.61	0.267	0.102	230	10.5
M01-06	8.58	0.316	0.094	230	9.60
M02-01	9.57	0.234	0.104	240	10.3
M02-02	7.29	0.195	0.075	220	7.92
M02-03	10.4	0.232	0.105	220	11.2
M02-04	10.1	0.231	0.102	220	10.8
M03	4.87	0.174	0.055	240	5.43
M04-01	6.25	0.157	0.066	230	6.76
M04-02	6.91	0.161	0.073	230	7.43
M05-01	6.40	0.077	0.065	230	6.65
M05-02	6.19	0.064	0.068	250	6.40
M05-03	6.42	0.071	0.066	240	6.65
M05-04	7.24	0.086	0.071	220	7.52
M06-01	9.72	0.193	0.106	240	10.3
M06-02	7.76	0.162	0.087	250	8.29
M06-03	9.43	0.185	0.100	240	10.0
M07-01	15.7	0.336	0.169	240	16.8
M07-02	15.6	0.319	0.160	230	16.6
M07-03	12.2	0.330	0.130	230	13.3
M07-04	9.99	0.265	0.114	250	10.8
M07-05	8.72	0.261	0.097	240	9.57
M07-06	9.35	0.269	0.102	240	10.2

Sample & Grain No.	ThO_2 (wt%)	UO_2 (wt%)	PbO (wt%)	t (Ma)	UO_2^* ThO_2^*
(No. 0401)					
Z01	0.087	0.495	0.018	250	0.522
Z02-01	0.643	1.18	0.044	240	1.38
Z02-02	0.204	0.815	0.029	240	0.878
Z02-03	0.367	1.00	0.034	230	1.11
Z02-04 R	1.64	1.23	0.040	170	1.74
Z02-05 R	1.96	1.51	0.047	160	2.12
Z03-01	0.255	0.910	0.035	260	0.989
Z03-02	0.260	1.32	0.049	260	1.40
Z03-03	0.611	1.38	0.053	250	1.57
Z03-04 R	1.15	1.67	0.044	160	2.03
Z03-05 R	1.70	2.18	0.059	160	2.71
Z04	0.093	1.15	0.036	230	1.18
Z04	0.306	0.892	0.032	240	0.986
Z04	0.143	0.850	0.029	240	0.894
(No. 0402)					
Z01	0.066	0.420	0.014	230	0.440
Z02	0.191	0.409	0.016	250	0.468
Z03	0.168	0.293	0.011	240	0.345
Z04-01	0.071	0.667	0.022	240	0.689
Z04-02	0.070	0.601	0.021	250	0.623
Z04-03	0.060	0.475	0.016	240	0.494
Z04-04	0.075	0.353	0.012	240	0.376
Z05-01 r	0.191	0.323	0.025	470	0.381
Z05-02 r	0.102	0.186	0.014	470	0.217
Z05-03 r	0.016	0.148	0.010	470	0.153
Z05-04 r	0.156	0.263	0.019	440	0.310
Z05-05 r	0.167	0.312	0.024	480	0.363
Z06-01	0.079	0.575	0.020	250	0.599
Z06-02	0.116	0.530	0.019	250	0.566
Z06-03	0.191	0.752	0.027	250	0.811

Appendix 2 (cont'd)

Sample & Grain No.	ThO_2 (wt%)	UO_2 (wt%)	PbO (wt%)	t (Ma)	UO_2* ThO_2*
(No. 0403A)					
Z01-01 r	0.185	0.388	0.026	420	0.444
Z01-02 r	0.112	0.324	0.020	410	0.358
Z02-01	0.126	0.423	0.016	260	0.462
Z02-02	0.091	0.351	0.013	250	0.379
Z03-01	0.132	0.476	0.017	240	0.517
Z03-02	0.176	0.428	0.016	240	0.482
Z03-03	0.187	0.462	0.017	240	0.520
Z04-01	0.144	0.593	0.019	220	0.638
Z04-02	0.216	0.522	0.021	260	0.589
Z05-01	0.294	0.807	0.030	250	0.898
Z05-02	0.433	0.888	0.035	250	1.02
Z06	0.252	0.648	0.024	240	0.726
Z07 r	0.146	0.499	0.031	410	0.543
Z08	0.130	0.556	0.021	260	0.596
Z09	0.101	0.350	0.013	250	0.381
A10	2.43	0.567	0.031	170	4.26
Z11-01 C	0.201	0.942	0.085	600	1.00
Z11-02 C	0.163	0.964	0.074	520	1.01
Z11-03 M	0.076	0.414	0.013	220	0.437
Z11-04 M	0.083	0.468	0.015	220	0.494
Z12-01	0.105	0.522	0.017	230	0.554
Z12-02	0.177	0.566	0.021	250	0.621
Z13-01	2.23	0.966	0.052	230	1.65
Z13-02	0.214	0.952	0.036	260	1.02
Z13-03	0.037	0.669	0.022	240	0.680
Z14	0.110	0.558	0.020	250	0.592
Z15	0.113	0.532	0.019	250	0.567
Z16	0.359	1.08	0.038	240	1.19
Z17	0.198	0.834	0.028	230	0.895
Z19	0.134	0.589	0.021	250	0.630
Z20	0.111	0.447	0.016	250	0.481
Z21	0.199	0.538	0.021	260	0.599

Sample & Grain No.	ThO_2 (wt%)	UO_2 (wt%)	PbO (wt%)	t (Ma)	UO_2* ThO_2*
(No. 2804)					
Z01	0.173	0.565	0.021	250	0.618
Z02	0.260	1.28	0.049	260	1.36
Z03	0.381	3.39	0.113	240	3.51
Z04	0.238	0.607	0.024	260	0.680
Z05	0.134	1.33	0.049	260	1.37
Z06	0.423	1.83	0.060	230	1.96
(No. 0403B)					
Z01	0.067	1.60	0.051	230	1.62
Z02-01 mR	0.148	2.50	0.063	180	2.55
Z02-02	0.119	1.29	0.043	240	1.33
Z02-03	0.139	2.11	0.059	200	2.15
Z02-04	0.095	1.29	0.043	240	1.32
Z03-01	0.395	3.98	0.138	250	4.10
Z03-02	0.277	2.05	0.068	240	2.14
Z04-01	0.078	1.21	0.039	230	1.23
Z04-02	0.190	1.87	0.058	220	1.93
Z04-03	0.507	9.06	0.294	240	9.22
Z04-04	0.812	3.07	0.103	230	3.32
A05-01	5.39	0.136	0.042	170	5.83
A05-02	17.2	0.546	0.110	140	19.09
A05-03	4.08	0.123	0.034	180	4.48
Z06-01	0.019	0.676	0.023	250	0.682
Z06-02	0.098	1.53	0.053	250	1.56
Z06-03	0.126	1.94	0.063	240	1.98
Z07-01 m	0.035	2.16	0.054	180	2.17
Z07-02 m	0.031	2.18	0.052	180	2.19
Z07-03 m	0.020	2.02	0.048	180	2.03
Z08-01	0.012	0.875	0.029	240	0.879
Z08-02 mR	0.196	3.51	0.091	190	3.57
Z08-03 mR	0.041	2.50	0.046	140	2.51

Appendix 2 (cont'd)

Sample & Grain No.	ThO_2 (wt%)	UO_2 (wt%)	PbO (wt%)	t (Ma)	UO_2* ThO_2*
Z08-04	0.014	1.18	0.038	240	1.18
Z09-01	0.148	3.20	0.098	220	3.25
Z09-02	0.022	1.12	0.039	250	1.13
Z09-03	0.040	0.664	0.022	240	0.676
Z10 r	0.092	1.49	0.143	670	1.52
Z11	0.144	4.29	0.121	210	4.33
Z12 m	0.554	13.7	0.387	210	13.9
Z13-01	0.025	1.71	0.053	230	1.72
Z13-02 R	0.051	2.64	0.066	180	2.66
Z14 m	0.030	4.90	0.063	100	4.91
Z15-01	0.039	2.19	0.075	250	2.20
Z15-02	0.058	2.17	0.072	240	2.19
Z16	0.013	0.587	0.020	250	0.591
Z17	0.172	2.46	0.084	250	2.51
Z18	0.689	1.91	0.067	230	2.12
Z19 R	1.35	2.58	0.069	170	3.00
(No. 0403C)					
Z01-01	0.038	1.00	0.032	230	1.01
Z01-02	0.062	1.20	0.038	230	1.22
Z01-03	0.401	7.29	0.233	230	7.41
Z01-04	0.043	1.17	0.037	230	1.18
Z02-01	0.029	0.572	0.019	240	0.581
Z02-02	0.060	0.654	0.022	240	0.673
Z02-03	0.014	0.623	0.020	240	0.627
Z03-01	0.028	0.615	0.020	240	0.624
Z03-02	0.077	1.57	0.051	240	1.59
Z03-03	0.035	0.451	0.015	240	0.462
Z04-01	0.455	6.42	0.225	250	6.56
Z04-02	0.307	6.88	0.226	240	6.97
Z04-03	0.227	5.06	0.173	250	5.13
Z04-04	0.066	0.970	0.032	240	0.990
Z04-05	0.309	5.45	0.186	250	5.55
Z05-01	0.043	1.95	0.062	230	1.96
Z05-02	0.081	2.94	0.092	230	2.97
Z05-03	0.063	2.55	0.080	230	2.57
Z05-04	0.040	1.86	0.056	220	1.87

Sample & Grain No.	ThO_2 (wt%)	UO_2 (wt%)	PbO (wt%)	t (Ma)	UO_2* ThO_2*
Z05-05	0.010	0.860	0.027	230	0.863
Z06-01	0.101	1.26	0.040	230	1.29
Z06-02	0.150	2.74	0.087	230	2.79
Z06-03	0.078	1.79	0.059	240	1.81
Z07	0.946	3.49	0.124	240	3.78
Z08	0.050	0.796	0.027	250	0.811
Z09-01 C	0.035	0.509	0.027	380	0.520
Z09-02 C	0.099	1.69	0.086	360	1.72
Z09-03 M	0.153	2.24	0.073	240	2.29
Z09-04 M	1.62	9.44	0.291	220	9.94
Z09-05 M	0.127	2.08	0.066	230	2.12
Z10-01	0.174	2.09	0.072	250	2.14
Z10-02	0.170	2.06	0.064	220	2.11
Z10-03	0.162	2.08	0.069	240	2.13
Z10-04	0.349	1.12	0.040	240	1.23
Z10-05	0.173	1.64	0.056	240	1.69
Z10-06	0.070	1.38	0.043	230	1.40
Z11-01	0.411	3.01	0.097	230	3.14
Z11-02	0.998	16.1	0.489	220	16.4
Z12-01	0.055	1.63	0.057	250	1.65
Z12-02	0.041	0.895	0.030	240	0.908
Z13-01	0.100	2.73	0.088	240	2.76
Z13-02	0.203	3.55	0.109	220	3.61
Z13-03	0.070	1.44	0.046	230	1.46
Z14-01	1.47	24.6	0.764	230	25.1
Z14-02	0.414	5.17	0.153	210	5.30
Z14-03	0.106	3.15	0.096	220	3.18
Z14-04	0.305	7.29	0.216	220	7.38
Z14-05	0.015	0.821	0.027	240	0.826
Z15	2.58	11.2	0.369	230	12.0
Z16	0.059	1.73	0.054	230	1.75
Z17-01	1.34	4.66	0.141	210	5.07
Z17-02	0.053	1.58	0.049	230	1.60
Z17-03	0.161	2.47	0.076	220	2.52
Z17-04	0.493	2.43	0.086	250	2.58
Z18-01 mR	0.466	6.85	0.174	180	6.99
Z18-02	0.239	3.64	0.112	220	3.71
Z18-03	0.126	2.60	0.084	230	2.64
Z18-04	0.235	4.18	0.135	230	4.25

Appendix 2 (cont'd)

Sample & Grain No.	ThO_2 (wt%)	UO_2 (wt%)	PbO (wt%)	t (Ma)	UO_2* ThO_2*
(No. 28001B)					
Z01-01	2.56	2.99	0.128	250	3.78
Z01-02	2.91	2.83	0.129	250	3.73
Z01-03 mR	6.10	4.63	0.163	190	6.52
Z01-04 m	6.90	5.35	0.237	230	7.48
Z01-05 m	5.80	3.94	0.192	250	5.73
Z01-06	1.13	2.29	0.079	220	2.64
Z01-07	3.41	2.48	0.121	250	3.53
Z01-08	2.40	2.14	0.092	240	2.88
Z02	0.278	1.03	0.034	230	1.12
Z03-01	0.419	1.19	0.038	210	1.32
Z03-02	0.511	1.13	0.040	230	1.29
Z03-03	0.225	1.34	0.047	250	1.41
Z03-04	3.93	3.26	0.145	240	4.47
Z03-05	1.11	0.870	0.035	210	1.21
Z03-06	0.150	0.462	0.016	230	0.508
Z04	0.396	1.40	0.046	220	1.52
Z05	0.322	0.987	0.037	250	1.09
Z06	3.10	3.19	0.135	240	4.15
Z06	0.084	1.33	0.041	220	1.36
Z07	1.48	1.88	0.075	240	2.34
Z08	4.99	4.32	0.196	250	5.86
Z09-01	4.73	4.11	0.181	240	5.57
Z09-02	0.722	1.30	0.051	250	1.52
Z09-03	2.50	3.02	0.126	240	3.79
Z09-04	1.93	2.39	0.094	230	2.99
Z10-01	0.082	0.862	0.028	230	0.887
Z10-02 R	0.448	1.22	0.032	180	1.36
Z11	3.99	3.74	0.156	230	4.97
Z12	2.24	3.20	0.119	230	3.89
Z13	0.421	1.34	0.050	250	1.47

Plate I

Occurrence of the Gray Granite as veins cutting the Hida gneiss at Futatsuya. Two veins of coarse-grained to pegmatitic granite (light gray in color) have intruded subconcordantly into the hornblende-biotite gneiss, and are in turn cut by a discordant vein of fine-grained quartz monzonite (gray in color). The 0701A sample was collected from the extension of the coarse-grained older veins, and 0701B sample from the fine-grained younger vein.

Plate II

Occurrence of the Gray Granite at Futatsuya, about 60 m downstream from the outcrop shown in Plate I. The Gray Granite (light gray in color) has agmatized the hornblende-biotite gneiss (dark gray in color). No reaction of the granite with the agmatized blocks is observed.

Plate III

Occurrence of the Gray Granite as light gray network veins at Kagasawa. This outcrop is the same as that described in Figs. 1 and 2 of Shibata and Nozawa (1986). They grouped the vein rocks into three; coarse-grained granite, medium-grained granodiorite and fine-grained granite in the order of intrusion.

Plate IV

A: Transmitted light photomicrograph of Z08 euhedral zircon grain with concentric growth zoning from 0701A sample at Futatsuya. Microprobe analysis shows the composition to be 32.3% SiO_2, 65.3% ZrO_2, 1.50% HfO_2, 0.020% ThO_2, 0.089% UO_2, 0.168% Y_2O_3 and 0.066% P_2O_5. The PbO content is less than 0.006%.

B: Transmitted light photomicrograph of Z03 rounded zircon grain from 0701A sample at Futatsuya. This grain contains 0.011% ThO_2, 0.043% UO_2 and a hardly detectable amount of PbO.

C: Transmitted light photomicrograph of Z01 zircon grain with a distinct core-overgrowth relation from 0702B sample at Futatsuya. The well-rounded core is mantled by a rim forming a euhedral outline. both the core and rim have the same optical orientation. The core contains hardly detectable amounts of ThO_2, UO_2 and PbO.

D: Transmitted light photomicrograph of M07 monazite grain from 1501B sample at Kagasawa. It is transparent under the microscope despite the high ThO_2 content (8.72-15.7%).

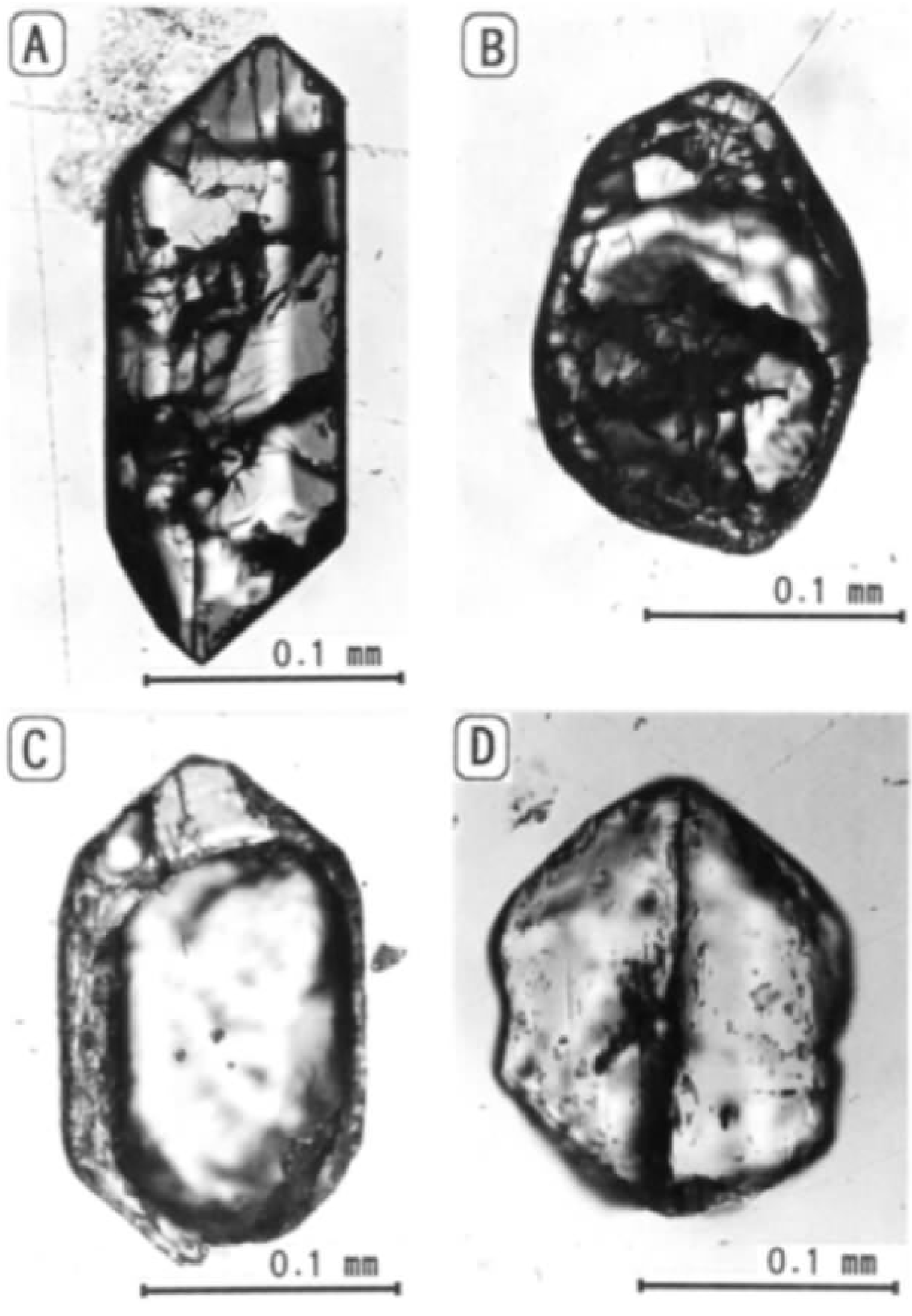
A
0.1 mm
B
0.1 mm
C
0.1 mm
D
0.1 mm

Plate V

A and B: Transmitted light (A) and reflected light (B) photomicrographs of Z16 zircon grain from 0702B sample at Futatsuya. Note a distinct core-overgrowth relation; the subrounded core is translucent owing to metamictization and is mantled by a euhedral rim with growth zoning. The CHIME age for the core is 500 ± 50 Ma (Fig.5).

C and D: Transmitted light (C) and reflected light (D) photomicrographs of Z01 zircon grain from 2801B sample at Amo, showing a clear concentric growth zoning. This grain contain 1.1-6.9 % ThO_2 and 2.1-5.4 % UO_2. Most parts are translucent owing to metamictization, but show a concordant PbO- UO_2* relation.

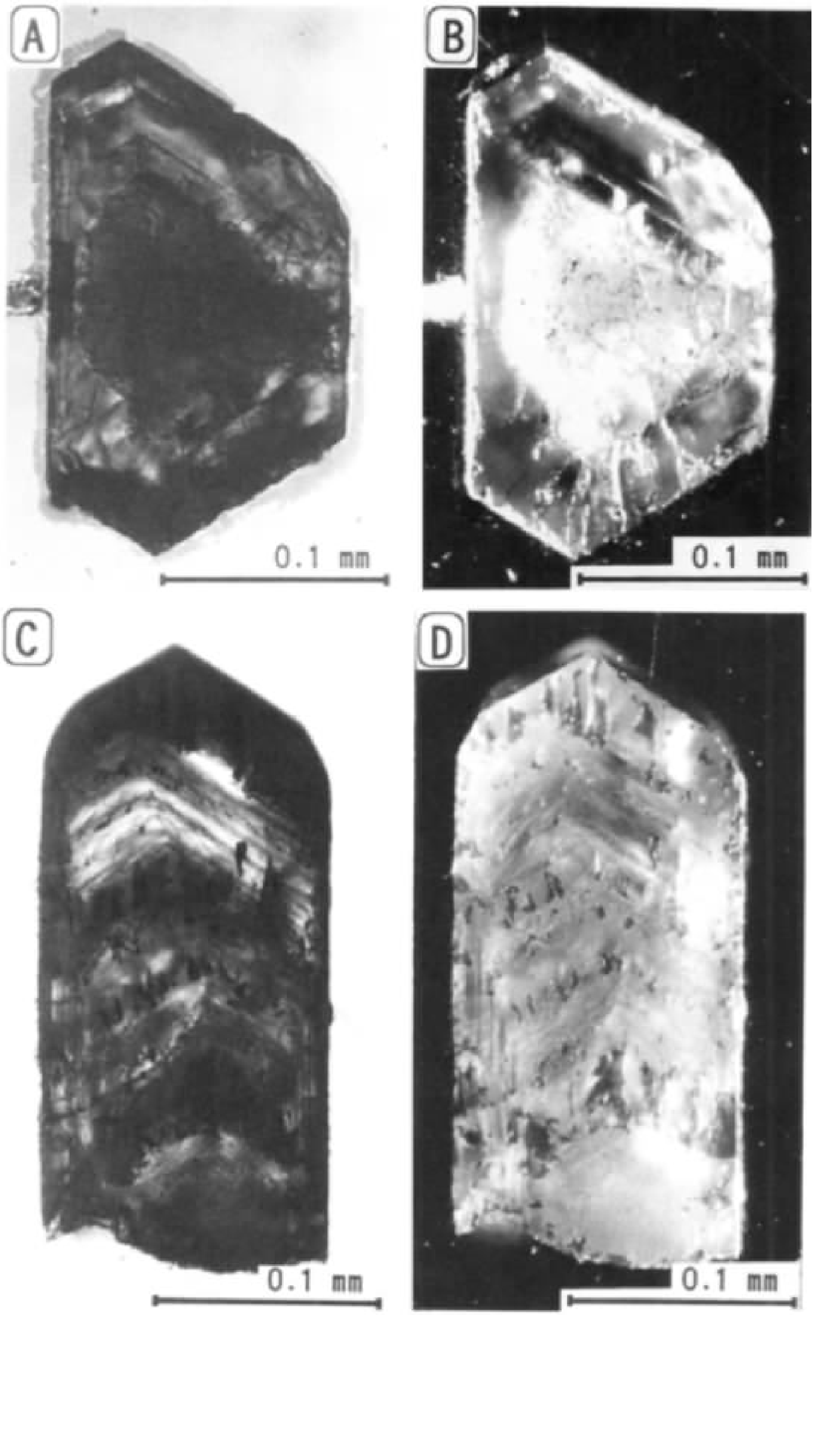
A
0.1 mm
B
0.1 mm
C
0.1 mm
D
0.1 mm